https://doi.org/10.1016/j.jclepro.2019.119269

Multi-criterion optimization of integrated photovoltaic facade with inter-building effects in diverse neighbourhood densities

Xi Chen[*a, b], Junchao Huang [b], and Hongxing Yang [b]

[a] School of Science and Technology, The Open University of Hong Kong, Kowloon, Hong Kong, China

[b] Renewable Energy Research Group (RERG), Department of Building Services Engineering, The Hong Kong Polytechnic University, Kowloon, Hong Kong, China

Abstract

Inter-building effects have been proved to have significant impacts on the energy and indoor environmental performance of adjacent building developments in densified urban environment. Therefore, this study presents a multi-criterion design optimization and decision-making approach for an integrated PV facade design considering miscellaneous inter-building factors as well as corresponding criteria specification in major green building assessment schemes. The impact of the surface reflectance and façade geometry is quantified for the lighting energy demand, HVAC energy demand, photovoltaic (PV) energy supply and indoor visual discomfort time respectively with a robust global sensitivity approach in diverse urban density scenarios. Wall reflection is determined to be the most important urban design factor contributing to 34% to 66% variation of different performance indicators as per the availability of solar radiation on different building surfaces. Multi-dimension parametric analyses and design optimizations of PV envelope design parameters are then conducted for different neighborhood densities with fixed surface properties of peripheral building facades. Sensitivity indices of window and shading design parameters are subject to significant variation when considering surface properties of peripheral buildings. Furthermore, the performance of two different decision-making strategies (i.e. Technique for Order of Preference by Similarity to Ideal Solution and Minimum Distance to the Utopia Point methods) is compared based on criteria weightings from green building assessment schemes. The final optimum solution closest to the ideal is then determined by two-dimensional charts of objective functions. The integrated design optimization considering peripheral reflection can change the estimated net energy demand

[*] Corresponding author e-mail: climber027@gmail.com; pchen@ouhk.edu.hk

by up to 8.84% (mainly in PV supply and lighting demand). These research findings can promote the integration of synergetic energy and indoor environment design strategies and expand the penetration of renewable applications in urban areas.

Keywords: Photovoltaic envelope; Energy demand; Visual discomfort; Multi-criterion optimization; Decision-making

1. Introduction

The energy consumption of buildings has been growing rapidly over the world in recent decades due to the increased requirement of the indoor environment quality (IEQ) and expanding population (Lam et al., 2004). Especially in large cities with high-population densities, buildings tend to dominate the primary energy consumption when the service industry is replacing the traditional manufacture industry. For instance, commercial and residential sectors in Hong Kong are responsible for over 90% electricity consumption as per statistics form the government (EMSD, 2018; Yu and Chow, 2001). Building energy codes and green building assessment schemes are therefore launched to improve the building energy efficiency while maintaining expected functional quality for occupancy (Marzouk et al., 2018). The improved energy efficiency is usually justified in a performance-based approach by comparing the energy use index of the designed scenario with that of the baseline/benchmarking scenario (BEAM, 2012). Peripheral buildings are not included in the energy use modelling as their influences are usually specified in other assessment categories, such as the site aspect, in a green building assessment scheme. However, such modelling approach can cause great deviation from the practical condition in a densified urban environment. Urban densification is currently considered as one of the feasible sustainable development strategy to solve contradictions between social, economic and environmental factors (Lima et al., 2019). The complicated inter-building effect caused by densification urges the integration of the assessed building into its neighbourhoods. Neighbourhood densities together with thermal and geometrical properties of peripheral building surfaces can influence the availability of solar radiation for the assessed building/project building by which its energy and indoor environmental performances are significantly changed (Peng et al., 2016).

The building envelope is the interface between the neighbourhood and indoor environment, accounting for 20-50% cooling and heating energy consumption (Lam, 2000; Zhang et al., 2016a).

For high-rise buildings, a judicious design of the building envelope (i.e. mainly vertical facades) can contribute to over 50% of the energy demand reduction in both thermal and lighting aspects (Chen et al., 2019b; Huang et al., 2018). Such an improvement of the envelope performance can be attributed to basic passive architectural design parameters in the layout, thermophysical, geometric and air-tightness aspects (Chen et al., 2019a; Sadineni et al., 2011). Especially, passive design parameters related to windows (e.g. the size, thermal/optical properties, shading and orientation) can regulate the amount of solar radiation penetrating the external building facade and greatly impact the indoor daylight and visual performance (Lee and Won, 2017; Li et al., 2006; Mangkuto et al., 2016). Besides traditional building envelope designs, innovative applications of building integrated photovoltaic (BIPV) windows and walls (Chan, 2018), also bring uncertainties and challenges for optimizing building facades (Baldi et al., 2015). Building envelope design optimizations are mostly conducted for simple-box hypothetical buildings (Delgarm et al., 2016) or stand-alone buildings with different dimensions and shapes (Zhang et al., 2017), whereas seldom integrated with peripheral urban contexts.

Four different surrounding urban contexts are considered for the building form optimization to improve daylight and natural ventilation performances in different climatic zones, but variation of urban densities and surface properties of peripheral buildings are only mentioned as recommendations for the future work (Konis et al., 2016). More detailed urban morphological factors are investigated for the sensitivity of available solar radiation on the vertical facades in a Brazilian building, while indoor environmental and energy performances are not covered in this research (Martins et al., 2016). The influence of three different urban densities and other confounding factors on building energy demands are estimated for both real and simplified urban morphologies of New York (Samuelson et al., 2016). This study proves a correlation between urban contexts and design decisions for building envelopes but lacks quantifiable sensitivity indices. Similarly, the annual average vertical daylight factor on building facades is predicted for three fundamental urban layouts, where the optimal layout is recommended for the cold climate of northeast China (Lu and Du, 2019). The thermal demand (i.e. cooling and heating load) of three urban district models is subject to sensitivity analyses for both urban morphological and building envelope parameters (Martins et al., 2019). The importance of design parameters is ranked as a reference for future optimization studies. Such an estimation of the neighborhood effect can be more accurate when coupled with urban-scale CFD modelling (Shen et al., 2019). Furthermore, both the solar harvesting potential and energy use are investigated by sensitivity analyses considering urban planning and building geometric parameters in Singapore (Zhang et al., 2019). The study suggests developing an integrated renewable application, passive design optimization and decision-making approach in future. However, none of the above-mentioned studies focus on the radiative heat exchange and corresponding inter-building effect (IBE) considering the surface reflectance. Its joint effect with the neighborhood shading on the building energy use is observed in a recent study on both generalized and realistic urban contexts (Han et al., 2017). The shading effect is found to be more important and the generalized 9-block building network is proved to be a reliable modelling approach to IBE. The impact of the radiative heat exchange between buildings on the cooling load is also investigated in an urban canyon scenario with different surface reflectance and canyon dimensions (Allegrini et al., 2016; Huang and Li, 2017). Both studies conducted building load predictions by coupled city-scale modelling and EnergyPlus, but more detailed surface geometric properties such as window sizes are not well addressed. Surface geometric and thermal properties (i.e. the window to wall ratio and solar reflectance) as well as urban densities are jointly investigated in a recent parametric study on a Brazilian office building. Nonetheless, the study only qualified their influences over the building thermal load without a global sensitivity approach (Lima et al., 2019).

Among the reviewed literatures, few studies have incorporated the design optimization of building envelopes with detailed peripheral urban environment especially concerning the radiative heat transfer dependent on surface geometric and thermal properties. Limited available studies usually fail to quantity the exact contribution of each design factor (urban or building) or ignore important performance indicators for sustainable building designs. To fill such research gaps, this study developed a synthetic sensitivity analysis and design optimization approach with robust decision-making strategies for photovoltaic (PV) envelopes under different urban contexts. Building energy demands are optimized together with the indoor environmental quality and solar harvesting potential. The Technique for Order of Preference by Similarity to Ideal Solution (TOPSIS) is compared with the Minimum Distance to Utopia Point (MDUP) to determine the final optimum solution from the Multi-criterion solution space. The influence of thermal and geometric parameters of peripheral building facades will be quantified by both global and local sensitivity analysis methods for diverse urban densities. In addition, the interactive effect of coupled PV and passive architectural design parameters is incorporated into the design optimization approach and the uncertainty of sensitivity indices regarding different neighborhood densities is examined.

2. Research design and methodology

Fig. 1 illustrates the overall framework of research methodology for this study. Two stages of global sensitivity analyses based on the Analysis of Variance (ANOVA) are conducted to quantify the impact of neighborhood building facade geometric and thermal parameters as well as PV envelope design factors in three urban density scenarios. Uncertainty of sensitivity indices for the integrated PV design is also evaluated against urban design factors. Finally, the building thermal and lighting demand, PV power generation potential and visual discomfort will be simultaneously optimized, while a multi-criterion decision-making strategy is developed to derive the optimum solution considering different objective weightings.

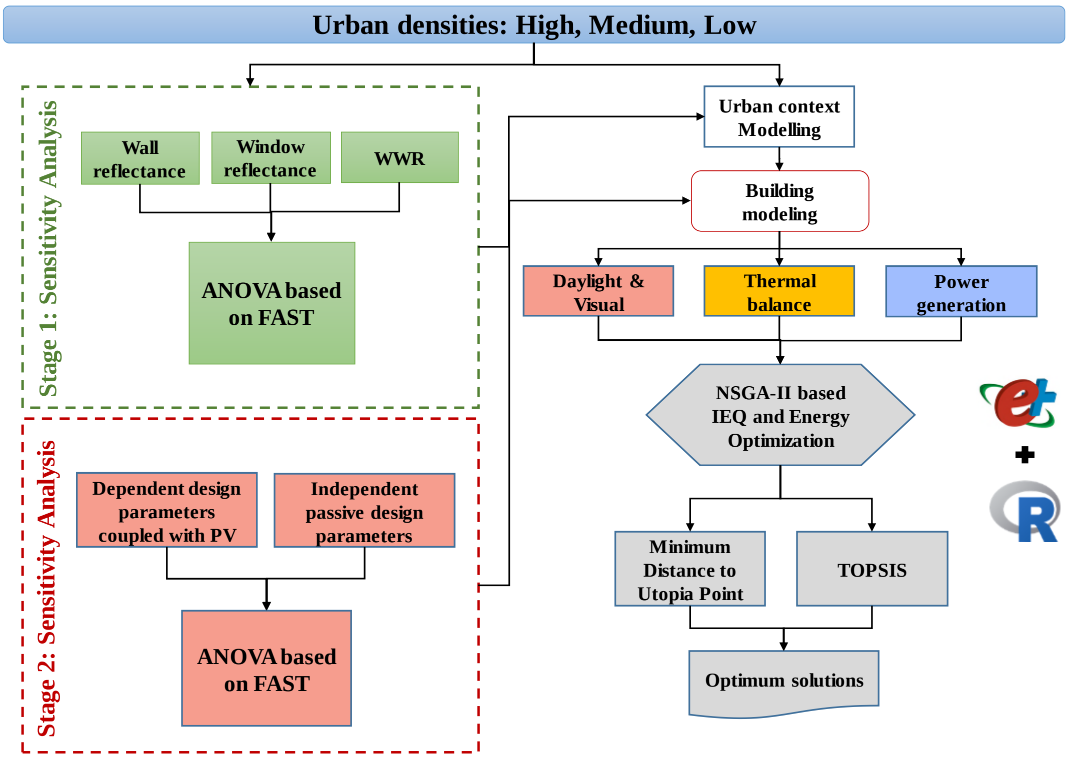

Fig. 1. Proposed overall research framework

2.1.Neighborhood urban context modelling

Urban context modelling is becoming more important for building performance assessments, as more research has proved its impact on the surrounded project building. Such impact can be summarized as the inter-building effect (IBE) mainly consisting of shading and reflectance related to the radiative heat transfer and daylight penetration. The local wind and thermal environment varied by large-scale urban morphologies is however not considered in this study, because their influences over a fully air-conditioned office building are not significant even in terms of the thermal load (Lima et al., 2019). The heat island effect and local environment will be addressed in future research where EnergyPlus is coupled with urban-scale simulation software such as CitySim and ENVI.

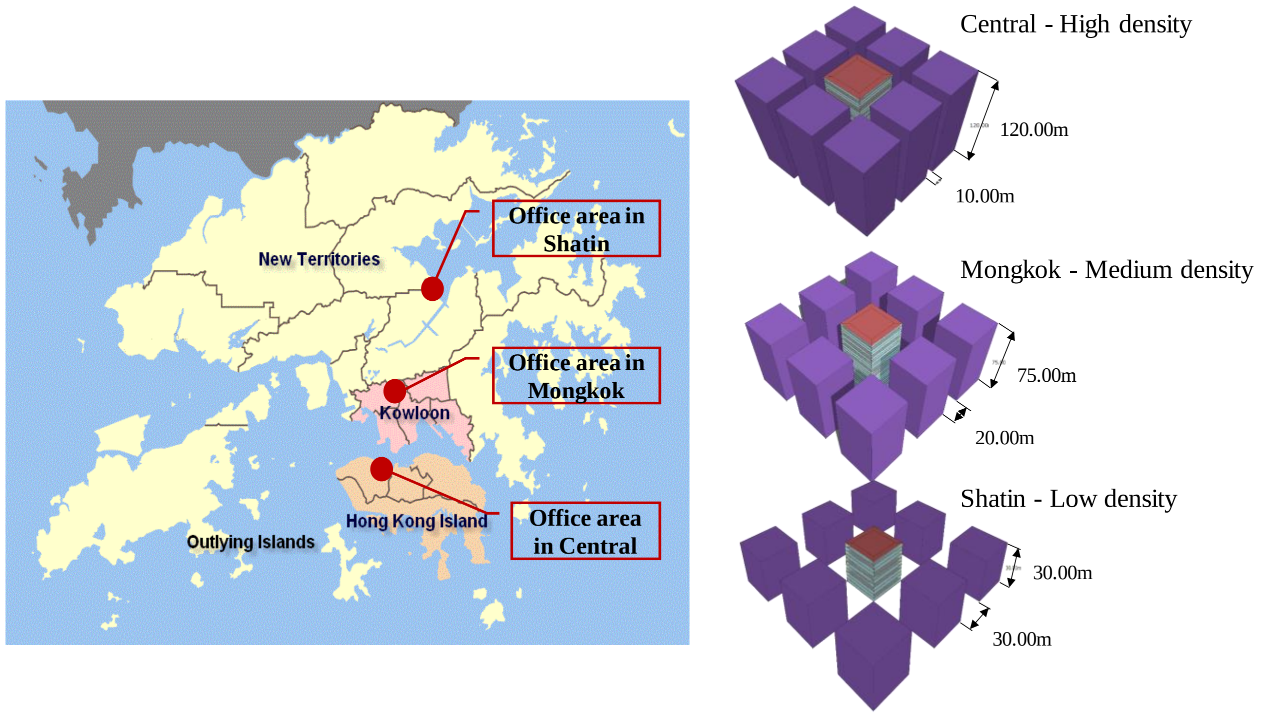

Fig. 2. Simplified urban blocks for selected commercial centres in Hong Kong (Chen et al., 2019b)

IBE is quantified for the investigated typical high-rise office building in three different density scenarios with simplified district block models. Unnecessary building surfaces are also removed from the model to increase computation efficiency while keeping reasonable accuracy as indicated in exiting studies (Chen and Hong, 2018; Han et al., 2017). Such simplification is also necessary for EnergyPlus modelling because too many overlapped shadows from peripheral shadings and inter-reflections could cause extensively more time for a single simulation run to reach convergence. Fig.

2 illustrates the high, medium and low-density scenarios for three major commercial districts in Central, Mongkok and Shatin across the whole territory of Hong Kong. A neighbourhood block with an average building height of 120m and a building height to street width ratio (H/W) of 12:1 is composed to represent the high-density context. A neighbourhood block with an average building height of 75m and an H/W of 3.75:1 is then representing the medium-density context. Finally, a neighbourhood block with an average building height of 30m and an H/W of 1:1 is representing the low-density context.

Table 1. Physical properties of peripheral building exterior surface

Design parameter	Value range	Medium level	Distribution
Window to wall ratio - WWR	0.10~0.83	0.47	Uniform, Continuous
Solar reflectance of walls – Ref_Wall	0.10~0.90	0.50	Uniform, Continuous
Solar reflectance of windows – Ref_Win	0.04~0.70	0.37	Uniform, Continuous

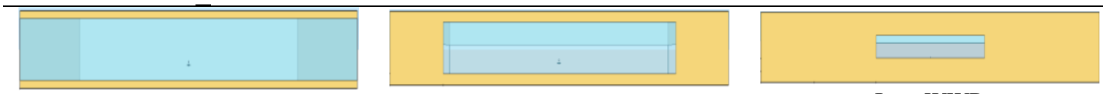

High WWR | Medium WWR | Low WWR

The building simulation setting in EnergyPlus has an important input item called "Solar Distribution", which regulates how direct and reflected solar radiation strikes building exterior surfaces and enters the internal zone. In this study, "FullExteriorWithReflections" is selected for "Solar Distribution" so that shadow patterns from all exterior surfaces (i.e. ground, building, shading) are addressed while all radiation penetrating the window is assumed to be falling on the floor. Redistributed radiation from the floor is then uniformly assigned to all other internal surfaces of the zone. Reflection calculations, although time-consuming in this mode, are fully executed for every external surface. Given the situation of closely populated high-rise buildings, reflectance from vertical facades should have the greatest impact on a typical floor. Therefore, reflectance from the exterior facades of peripheral buildings is evaluated with the following parameters as defined in Table 1. For opaque surfaces such as walls, the solar reflectance varies between 0.1 and 0.9 to represent complete-diffusive surfaces. The upper limit of 0.9 represents a whitewashed exterior furnish or other advanced high-reflectance materials (Burg et al., 2017), while the lower limit of 0.1 represents a black paint or absorptive materials like PV panels (Cha et al., 2018). Diffusive visible reflectance of the wall covariates with diffusive solar reflectance. The window to wall ratio (WWR) of peripheral buildings varies between 0.1 and 0.83, assumed to be of the same distribution as the surrounded project building. Reflectance of the outer layer of windows is changed between 0.04 and 0.70 in this study based on an a constant solar absorptance of 0.06 (Connelly et al., 2017; Selj et al., 2011). The total available solar gain as a combination of direct and diffusive radiation is obtain from Eq. (1) without IBE:

$$Q_{sol} = \alpha(I_b \cos\theta \frac{S_s}{S} + I_s F_{ss} + I_g F_{sg}) \quad (1)$$

where α is the solar absorptance of the surface; θ is the incidence angle of sun rays; S is the area of the surface; S_s is the sunlit area; I_b is the intensity of direct radiation; I_s is the intensity of sky diffusive radiation; I_g is the intensity of ground reflected diffuse radiation; F_{ss} is the angle factor between the surface and the sky; and F_{sg} is the angle factor between the surface and the ground.

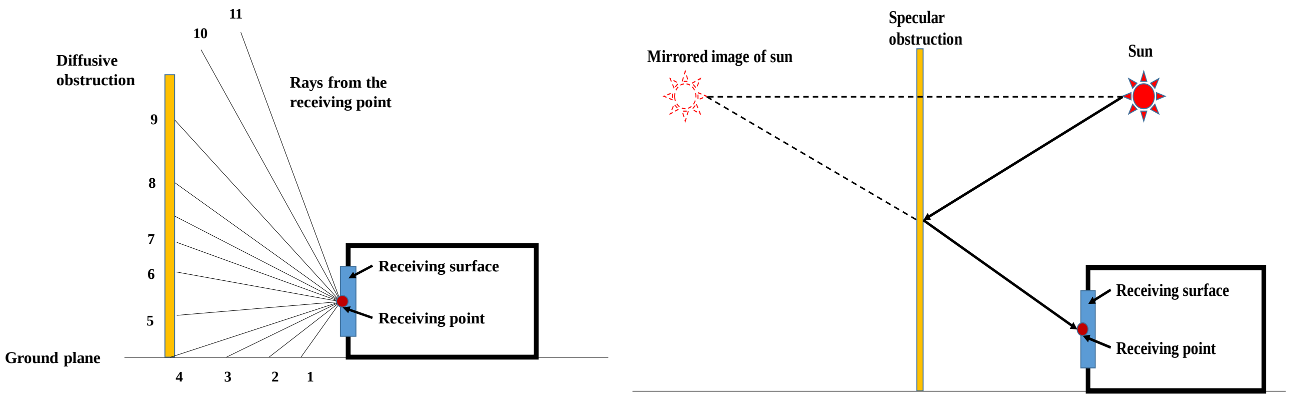

Fig. 3. Comparison of diffusive and specular reflection based on different obstruction surface properties

Apart from ground reflections, those from shadowing surfaces (i.e. peripheral buildings and overhangs) and building external surfaces (i.e. other surfaces of the project buildings) are also included to fully address IBE. Reflected solar radiation is classified as diffusive reflection by non-glazing surfaces (e.g. walls) and specular reflection by glazing surfaces (i.e. windows). The "FullExteriorWithReflections" option also calibrates the ground reflectance item in Eq. (1) to model an obstructed ground surface by buildings. Ray-tracing method is used in EnergyPlus to calculate diffusive reflection of beam and sky solar radiation reaching exterior surfaces (i.e. receiving surfaces) of the project building (Han et al., 2017). A set of rays is tracked from a given number of receiving points on the receiving surface, while the contribution of each ray to the receiving surface is determined if it hits an obstruction. The factor of diffusive reflection from peripheral buildings to the surface of the project building is then calculated separately for beam and sky solar radiation by subroutines of EnergyPlus. The factor of specular reflection for beam solar radiation from obstructions is however calculated in a different way compared to diffusive reflection as illustrated in Fig. 3.

2.2.Building modelling and performance criteria

On top of constructed neighborhood contexts in different commercial sectors of Hong Kong, a prototype 40-story high-rise office building is incorporated to model the whole building network as illustrated in Fig. 4 (Chan et al., 2009; Samuelson et al., 2016). The typical floor of the project building is characterized by four perimeter zones and one core zone with a dimension of 36m (length) * 36m (width) * 3m (height). The weather profile in the IWEC format from the City University of Hong Kong is adopted to predict building performances in a hot and humid climate, where both solar harvesting and passive architectural design strategies have many potential applications.

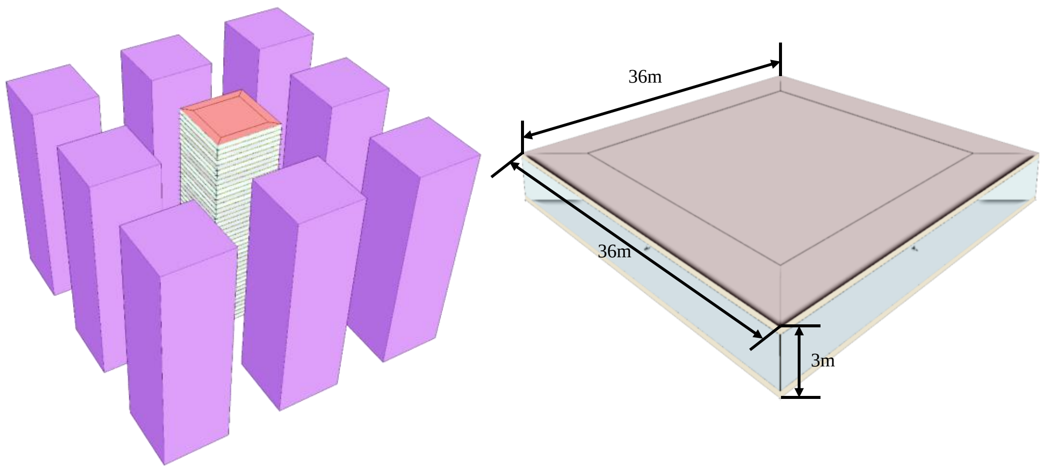

Fig. 4. Simplified building network and typical layout plan

Passive architectural and PV envelope designs are characterized by independent and dependent variables, in which independent variables are subject to the Fourier Amplitude Sensitivity Test (FAST) and multi-criterion optimization based on specified distribution functions as per Table 2.

Independent input parameters (i.e. the first 9 variables in Table 2) are defined to address building layout, thermophysical, geometrical and air-tightness aspects of the passive design (Chen et al., 2017b), which has been proved to greatly impact building thermal and lighting performances (Chen et al., 2017a; Gueymard and duPont, 2009). These nine design inputs are selected based on extensive literature reviews and multiple screening-based/variance-based sensitivity analyses for both residential and commercial developments when the inter-building effect is not considered (Chen et al., 2019a; Huang et al., 2018). Dependent design parameters, on the other hand, are defined to incorporate PV related parameters with the passive design. The solar heat gain coefficient and PV coverage of windows are derived from Eq. (2)-(3) and the coefficient of 0.9 refers to a visible transmittance of 90% for the transparent part of windows. The PV coverage of opaque walls is also assumed to be maximized as 90% (See Fig. 5).

Table 2. Building modelling parameter setup

	Item/parameters	**Setting**
Variable	Building orientation - BO (°)	0~180°, baseline = 0
	Wall specific heat - WSH (J/kg·K)	800~2000, baseline = 840
	Window visible transmittance - VT	0.24~0.9, baseline = 0.786
	Wall thermal resistance - WTR (m^2·K/W)	0.09~6.25, baseline = 0.136
	Light-to-solar gain ratio - LSG	1.0~2.4, baseline = 1.118
	Window to wall ratio - WWR	0.1~0.8, baseline = 0.833
	Window U-value - WU (W/m^2·K)	0.2~6, baseline = 2.63
	Overhang projection fraction - OPF *(Shading devices for all windows: length = window width; depth = window height*OPF; material = concrete)*	0.0~0.6, baseline = 0.0
	Infiltration air change per hour - IACH	0.05~1.5, baseline = 0.6
	Solar heat gain coefficient - SHGC	$SHGC = \frac{VT}{LSG} = \tau + \alpha p$ (2)
	(Active) Glazing PV area - GPVA	$GPVA = 1 - \frac{VT}{0.9}$ (3)
Constant	Occupancy	8 m^2/person
	Activity level	120 W/person
	Lighting gain	12 W/m^2
	Illuminance setpoint	300 Lux
	Dimming control	Continuous/Off
	Equipment gain	10 W/m^2
	HVAC system	IdeaLoadsAirSystem
	Cooling Setpoint	24/30 ℃
	Heating Setpoint	15.6/21 ℃
	Outdoor air flow	0.008 m^3/s·person

Note: τ is the directly transmitted solar radiation through the window; α is the absorbed solar radiation by the window panel; and p is the proportion of absorbed solar radiation which is eventually transferred to the indoor ambiance.

Besides the setting of above envelope design parameters, internal load and miscellaneous building system parameters are fixed and subject to constant operation schedules throughout the sensitivity and optimization analyses with reference to local and international building energy codes (2013; Nabil and Mardaljevic, 2006). These modelling inputs are fed into different subroutines of EnergyPlus to predict the daylight, visual, thermal and power generation performance of the project building within each urban context scenario.

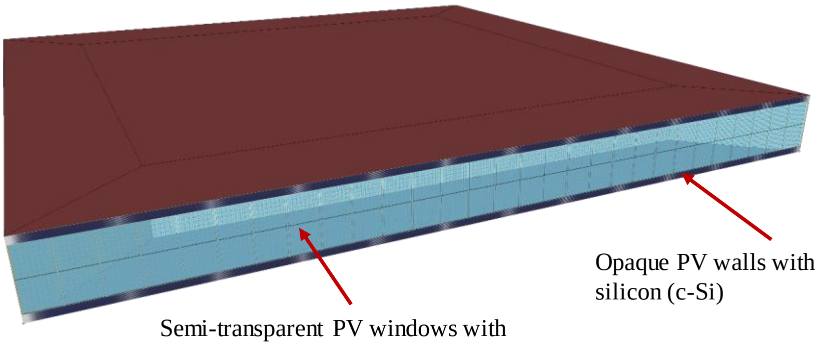

Fig. 5. Indication of PV configuration on vertical facades

2.2.1. Daylight and visual performance

Daylight calculations are performed in each simulation time step together with thermal balance modelling whenever the sunlight is available. Two reference points are located in the center of perimeter zones, one at 0.85 m as a typical working plane height for the daylight illuminance level and the other at 1.2 m as a typical eye level of seated occupants for the glare index.

The illuminance level at the reference point is derived from multiplying the exterior horizontal illuminance as per Eq. (4) at an unobstructed outdoor plane by the daylight factor as per Eq. (5) for the instantaneous solar position and sky condition. It is a combination of direct radiance through the window and reflected radiance from internal surfaces. A reference illuminance level of 300 Lux is set for office general task areas according to CIBSE Code of Lighting to perform the dimming control of auxiliary artificial lighting. No light dimming control is applied to internal core zones more than 4.6 m from the window due to the limited daylight access.

$$E_{h,sun} = \eta_{dir} S_{norm,dir} \cos Z \quad (4)$$

$$\bar{d}_{sun}(i_L, i_S) = w_j d_{sun}(i_L, i_S, i_h) + (1 - w_j) d_{sun}(i_L, i_S, i_h + 1) \quad (5)$$

where Z is the solar zenith angle; η_{dir} is the luminous efficacy of direct radiation from the sun; i_L is the reference point index; i_S is the window shade index (1 for unshaded windows); i_h is the hour number; and w_j is the weighting factor for the time-step interpolation.

The electrical lighting control system is then modelled to obtain the fractional lighting demand to meet the difference between the illuminance set point I_{set} and the daylight illuminance at the reference point I_{tot} by Eq. (6):

$$f_L(i_L) = \max\left[0, \frac{I_{set}(i_L) - I_{tot}(i_L)}{I_{set}(i_L)}\right] \quad (6)$$

"Continuous/off dimming control" is applied in this study, where the electric lighting should be able to meet I_{set} at the reference point in its rated condition, while the fractional lighting power f_P adjusted by f_L is calculated by Eq. (7). The lighting power reduction is further coupled with the calculation of zone thermal loads to reduce heat gains from luminaries. The adjusted lighting power for each time-step is then summed up through the typical meteorological year to predict the annual lighting demand.

$$f_P = \begin{cases} 0 & for: f_L < f_{L,\min} \\ \dfrac{f_L + (1 - f_L) f_{P,\min} - f_{L,\min}}{1 - f_{L,\min}} & for: f_{L,\min} \le f_L \le 1 \end{cases} \quad (7)$$

Glare index at the reference point is calculated with reference to the contrast between the window and background illuminance as per Eq. (8).

$$G_I = 10 \log\left(\frac{L_w^{1.6} \Omega^{0.8}}{L_b + 0.07 \omega^{0.5} L_w}\right) \quad (8)$$

where L_w is the average luminance of the window as seen from the reference point; Ω is the solid angle subtended by window; and L_b is the luminance of the background area. A threshold glare index of 22 is adopted in this study and the annual setpoint exceeded time is summed up and averaged over the four perimeter zones as the visual discomfort time.

2.2.2. Thermal demand and power generation

The zone thermal balance is approached with a predictor-corrector method in EnergyPlus by summing up the internal latent load, infiltration, air system, multi-zone airflow and convection with zone surfaces. The zone air temperature T_z is expressed by Eq. (9) and the humidity ratio is calculated in a similar pattern.

$$\rho_a C_p C_T \frac{dT_z}{dt} = \sum_{i=1}^{N_l} Q_i + \sum_{i=1}^{N_{surf}} h_i A_i (T_{si} - T_z) + \sum_{i=1}^{N_{zone}} m_i C_p (T_{zi} - T_z) + m_{\inf} C_p (T_\infty - T_z) \qquad (9)$$

where A_i is the area of room surfaces; C_p is the zone air specific heat; C_T is the sensible heat capacity multiplier; h_i is the convective heat transfer coefficient; m_i is the inter-zone air mass flow rate; m_{inf} is the infiltration air mass flow rate; N_l is the number of latent internal loads; N_{surf} is the number of zone surfaces; N_{zone} is the number of zones; Q_i is the convective internal load; T_{si} is the temperature of zone surfaces; T_{zi} is the mean temperature of i^{th} zone; T_∞ is the temperature of the outdoor air; and ρ_α is the zone air density.

ZoneHVAC:IdealLoadsAirSystem is adopted as a simplified ideal heating, ventilation and air-conditioning (HVAC) system to meet thermostat setpoints as specified in Table 2. The supply air temperature is determined based on the pre-defined supply air flow and the obtained zone air temperature from Eq. (9). The total supplied cooling and heating energy is then summed up through the year whenever the HVAC system is turned on.

When calculating power generation of integrated PV panels, the “Simple” generator model is adopted to provide a swift estimation of the solar energy harvesting potential of vertical façades based on Eq. (10). A constant average module conversion efficiency η_c of 6.3% and 15% is assumed for the amorphous silicon and monocrystalline silicon PV module respectively for window and wall applications (Wang et al., 2017; Zhang et al., 2016b). PV modules are also interacting with thermal balance calculations by selecting the “IntegratedSurfaceOutsideFace” option in the power generator’s setting (Chan, 2018).

$$P = A_s \cdot f_a \cdot G_T \cdot \eta_c \cdot \eta_i \qquad (10)$$

where A_s is the area of a PV surface; f_a is the fraction of the surface with active PV cells; G_T is the incident solar radiation on the vertical surface; and η_i is the conversion efficiency of the inverter. The power generation is then summed up throughout the typical year as the annual PV energy supply.

2.3.Sensitivity analysis and design optimization

To quantify the influence of urban contexts and building envelope design parameters over energy and indoor environmental performance indicators, the variance-based sensitivity method is adopted to address any non-linear and non-additive relationships between model inputs and outputs. The sensitivity analysis (SA) is first applied to urban context factors while building envelope factors are fixed to baseline/reference values. Both local and global SA approaches are used to highlight the impact of neighbourhood building geometric and thermal properties on all selected performance indicators. Then all urban context factors are fixed to their medium levels, so that the sensitivity of building performance indictors to the varied envelope design can be further explored. For all design factors, the uncertainty of sensitivity indices to three urban density scenarios is examined separately for a judicious site selection and building setback design.

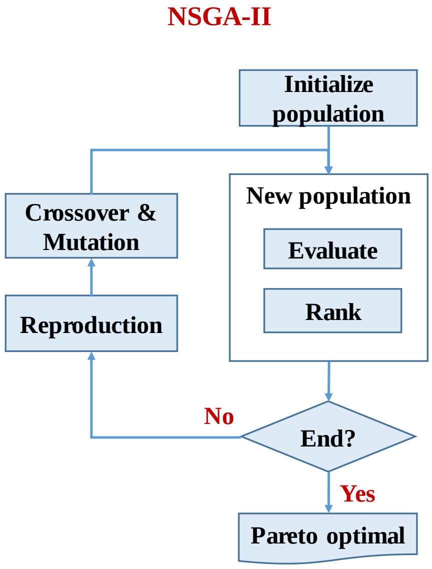

Parameter	Value
Population size	20
Number of generations	100
Crossover probability	0.9
Mutation probability	0.355
Tournament size	2

Fig. 6. Flowchart and setting of NSGA-II

The variance of building performance indicators can be demonstrated as:

$$V(Y) = \sum_{i=1}^{k} V_i + \sum_{j>i}^{k} V_{ij} \cdots + V_{12\cdots k} \tag{11}$$

where V_i is the unique impact of each design factor on the performance indictor, and V_{ij} is the superposed impact of any two design inputs. Different orders of sensitivity indices can then be derived as:

$$1 = \sum_{i=1}^{k} S_i + \sum_{j>i}^{k} S_{ij} + \cdots + S_{12\cdots k} \tag{12}$$

where S_i is the first-order sensitivity index to express the unique contribution of each design factor. S_{Ti} is then summed up as the total-order sensitivity index of a specific design factor:

$$S_{Ti} = S_i + \sum_{j \neq i}^{k} S_{ij} + \cdots + S_{i \cdots j \cdots k} \tag{13}$$

FAST (Fourier Amplitude Sensitivity Test) is used as the variance-based SA method in this study. It conducts a multi-dimensional transformation of the design space by changing factor x_i to a scalar $-\infty < s < +\infty$ as per Eq. (14) with a required number of building simulations as per Eq. (15)

$$x_i = \frac{1}{2} + \frac{1}{\pi} \arcsin(\sin(\omega_i s + \varphi_i)) \tag{14}$$

$$N = 2M\omega_{\max} + 1 \tag{15}$$

where M is the number of harmonics set to 4; ω_{max} is the maximum value among frequencies ω_i set as per (Cukier et al., 1978; Saltelli et al., 1999).

After quantifying the influence of urban contexts and envelope design parameters, the building lighting demand, HVAC demand, PV energy supply and visual discomfort time are subject to multi-criterion optimizations with a parametric design tool of EnergyPlus. Trade-offs between different optimization objectives can be observed from the Pareto Frontier obtained with the non-dominated sorting genetic algorithm-II (NSGA-II). NSGA-II reproduces and maintains a prescribed population size based on the non-dominated ranking mechanism and the crowding distance measure (See Fig. 6) (Pal et al., 2017). The population size, mutation and crossover probability as well as the tournament size are defined according to previously conducted adaptive optimization studies to ensure the convergence within a reasonable number of generations and balance between the exploitation and exploration of the design space (Chen et al., 2018). Post-optimization analyses and decision-making strategies are then applied to derive the final optimum solution for different urban context scenarios.

2.4. Multi-criterion decision-making approaches

A previous study conducted by the authors has adopted the Minimum Distance to the Utopia Point (MDUP) method and proved its advantage over the weighted sum method in delivering the optimum solution. MDUP starts with obtaining the Utopia Point, which is defined by minimizing each objective irrespective of other objectives. Such minimized objectives contribute to the coordinate of the Utopia Point, which is then normalized together with Pareto solutions so that all distances are compared in the same scale. The optimum solution is consequently determined based on the proximity between Pareto solutions and the ideal solution (i.e. Utopia Point).

Using the optimum solution from MDUP as the benchmark, another decision-making approach using TOPSIS (Technique for Order of Preference by Similarity to Ideal Solution) is proposed to determine the final optimum design solution based on diverse weighting schemes. Three weighting schemes will be examined in this study: (1) an equal weighting scheme without special emphasis on any objective; (2) a BEAM Plus based weighting scheme by summing up all relevant credits available in BEAM Plus - New Buildings for each objective; (3) a LEED based weighting scheme by summing up all relevant points available in LEED - Building Design and Construction for each objective. TOPSIS is a robust multicriteria decision-making approach to select the solution closest to the positive ideal solution and farthest from the negative ideal solution (Delgarm et al., 2016). It starts with constructing a decision matrix M with n design alternatives (within the Pareto Frontier) and the four performance assessment criteria. The intersection of each criterion and alternative is denoted as x_{ij} representing the rating of alternative A_i by criterion C_j:

$$M = \begin{bmatrix} & C_1 & C_2 & C_3 & C_4 \\ A_1 & x_{11} & x_{12} & x_{13} & x_{14} \\ A_2 & x_{21} & x_{22} & x_{23} & x_{24} \\ \vdots & \vdots & \vdots & \vdots & \vdots \\ A_n & x_{n1} & x_{n2} & x_{n3} & x_{n4} \end{bmatrix} \quad (16)$$

Then, the decision matrix is normalized by the following equation:

$$r_{ij} = \frac{x_{ij}}{\sqrt{\sum_{i=1}^{i=n} x_{ij}^{2}}} \quad (17)$$

The normalized matrix is denoted as $N = [r_{ij}]_{n\times 4}$, which will be further multiplied by $W=[w_i]_n$ and transferred into a weighted matrix $V=[v_{ij}]_{n\times 4}$. w_i is the weighting for each design criterion. The optimal solution S^+ and worst solution S^- are then determined as:

$$S^+ = \{v_1^+, v_2^+, v_3^+, v_4^+\} = [\max(v_{ij}), i \in I \mid \min(v_{ij}), j \in J] \quad (18)$$

$$S^- = \{v_1^-, v_2^-, v_3^-, v_4^-\} = [\min(v_{ij}), i \in I \mid \max(v_{ij}), j \in J] \quad (19)$$

where I is the indicator of a benefit criterion; and J is the indicator of a cost criterion.

Distances from the optimal solution/positive ideal solution S^+ and worst/negative ideal solution S^- are then determined as d_i^+ and d_i^-. Accordingly, the final optimum solution is obtained based on the ranking of a relative proximity of R_i. A larger R_i refers to a solution more approximate to the positive ideal solution and more favorable in decision-making.

$$d_i^+ = \sqrt{\sum_{j=1}^{4}\left(v_{ij} - v_j^+\right)^2} \, (i = 1, 2, \cdots, \mathrm{n}) \tag{20}$$

$$d_i^- = \sqrt{\sum_{j=1}^{4}\left(v_{ij} - v_j^-\right)^2} \, (i = 1, 2, \cdots, \mathrm{n}) \tag{21}$$

$$R_i = \frac{d_i^-}{d_i^- + d_i^+} \tag{22}$$

TOPSIS optimum solutions with different weighting schemes are compared with the solution by MDUP on two-dimensional charts of pared two objectives based on their proximity to the Utopia Point. Solutions closest to the origin of coordinates in the majority of these charts are determined as the final optimum.

3. Results and discussions

This section analyzes the influence of neighborhood building surface properties over building energy and daylight performance indicators and the uncertainty of envelope design sensitivity indices under different urban density scenarios. Different decision-making strategies are then combined with multi-criterion design optimizations to discuss the optimum PV envelope design in diverse urban contexts.

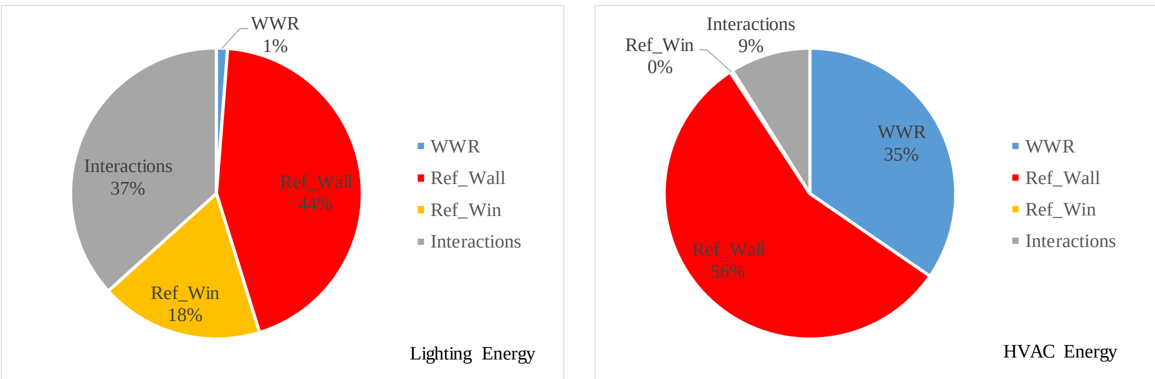

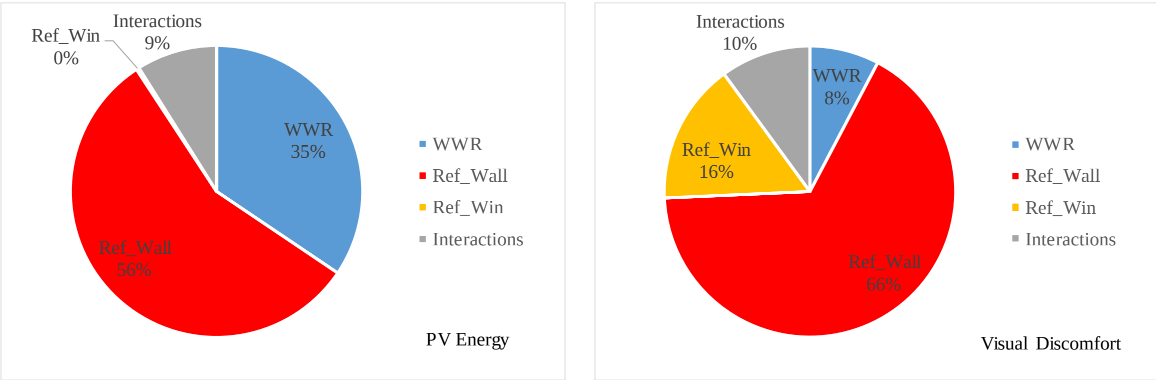

Fig. 7. Impact of peripheral building surface properties in the low-density case

Table 3 Variation of performances in local sensitivity analysis for the low-density scenario

	Lighting Energy Demand (kWh/m^2)	HVAC Energy Demand (kWh/m^2)	PV Energy Supply (kWh/m^2)	Visual Discomfort Time (hr)
Baseline	22.38	195.44	4.58	5764.00
Low WWR	22.38	199.64	4.87	6086.50
High WWR	22.39	191.44	4.28	5473.75
Low Ref_Win	22.40	195.04	4.55	5279.00
High Ref_Win	22.37	195.83	4.61	6149.50
Low Ref_Wall	22.41	190.33	4.20	5060.75
High Ref_Wall	22.37	200.64	4.95	6482.25

3.1.Sensitivity analysis for urban design factors

In the low-density urban context shown in Fig. 7, solar reflectance of walls (Ref_Wall) contributes to around 44% of the variation in the lighting energy demand, while the window to wall ratio (WWR) and solar reflectance of windows (Ref_Win) contribute to 1% and 18% of the output variation. The interaction between these three urban design factors, however, accounts for 37% of the variation. For the HVAC demand (mainly consisting of the cooling demand), the wall reflectance still contributes to the highest output variation of 56%, while the window to wall ratio and interactions contribute to 9% and 35% of the variation respectively. The window reflectance barely has any unique impact on the cooling demand. For the converted solar energy by PV facades, the same sensitivity result is obtained as for the HVAC energy demand. Regarding the visual discomfort, the contribution of wall reflectance reaches up to 66%, while the contribution of window reflectance also grows conspicuously to 16%. On the contrary, the contribution of WWR is reduced to 8%. Surface reflectance (i.e. the sum of Ref_Wall and Ref_Win) has a higher influence on building energy and lighting performance indicators than the window to wall ratio, which is consistent with the finding from a local sensitivity analysis conducted for a Brazilian office building (Lima et al., 2019). It can also be observed that diffusive reflectance by wall surfaces has a larger impact than the specular reflectance by window surfaces. Furthermore, a local sensitivity analysis is carried out by changing one of the three urban design factors to another level at a time while keeping other factors at the medium level. From a pairwise comparison in Table 3, the lighting energy demand shows no significant change with different levels of urban design factors, while the HVAC energy demand shows a minor variation of 2.66% when changing the wall reflectance. The PV energy supply and visual discomfort time, in contrast, have been changed by up to 8.14% and 12.46% with different wall reflectance levels. These minor differences are attributed to the relatively longer distances between the project and peripheral buildings, which impaired the radiative heat transfer.

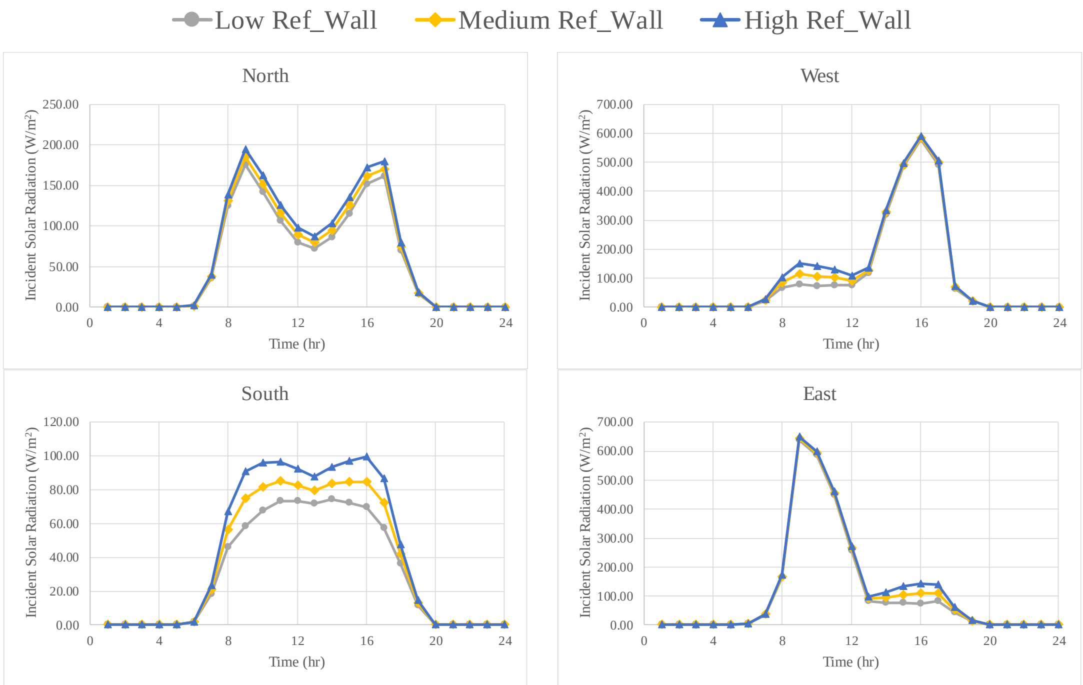

Fig. 8. Solar irradiance of project building facades for different wall reflectance of surrounding buildings with low urban density in a selected sunny day

Given the fact that all concerned building performance indicators in this study are related to available solar radiation, its distribution on each building façade is presented in Fig. 8 to highlight the impact of the most important urban design factors - wall reflectance – as identified from above sensitivity analyses. Incident solar radiation on the north façade is slightly higher than that on the south facade, as the selected sunny day is in mid-July when the sun is slightly to the north of Hong Kong. However, it is subject to less variation with wall reflectance compared to the south façade because reflected radiation mainly comes from the north facade of neighborhood developments.

East and west facades harvest more radiation in peak hours of the morning and afternoon. Nevertheless, reflection from the opposite peripheral building contributes to the fluctuation of solar irradiance with different wall reflectance levels on these two facades in reversed time sessions of the selected sunny day. From the comparison of solar radiation on different facades, it can be validated that wall reflectance is generally more influential on the solar harvesting potential because diffusive radiation has a greater opportunity to reach vertical building façades irrespective of solar altitude angles. On the contrary, specular reflectance from windows can only reach vertical façades of the project building in particular solar altitude angles and corresponding incident irradiance angles as per Fig. 3. Due to similar reasons, the window to wall ratio that determines the proportion of diffusive and specular reflection, is identified as the second important factor for varying the solar harvesting potential.

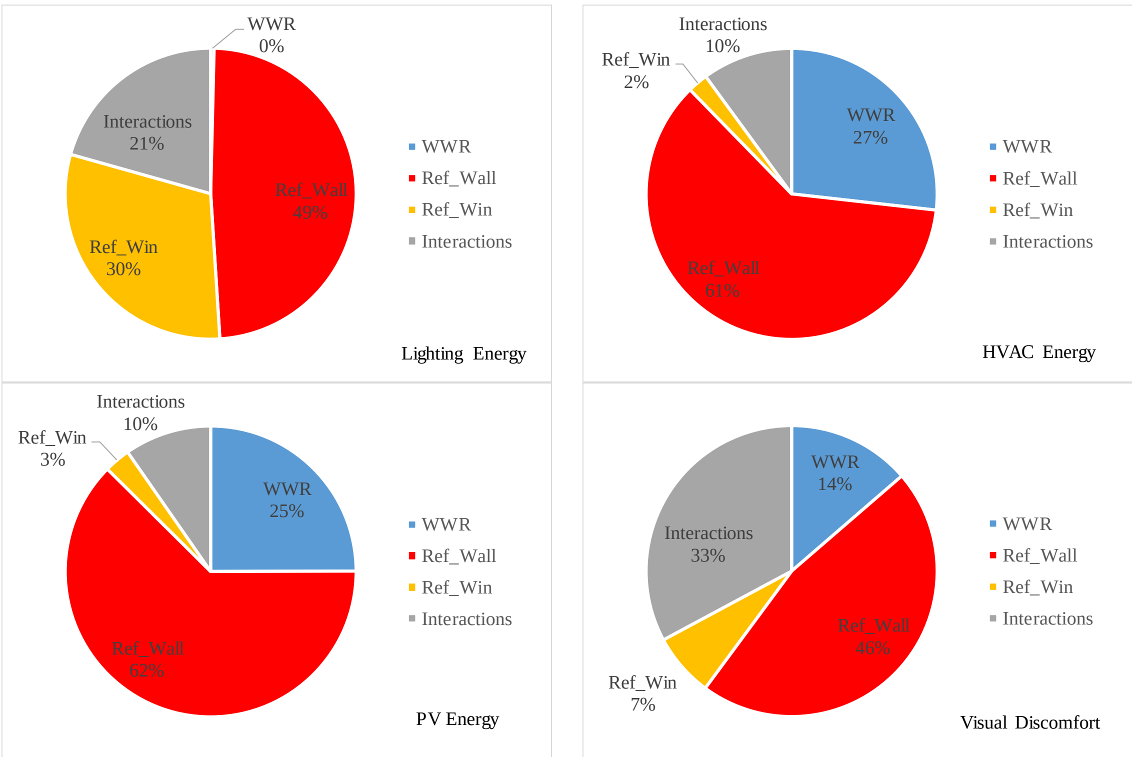

Fig. 9. Impact of peripheral building surface properties in the medium-density case

In the medium-density urban context as shown in Fig. 9, the contribution of Ref_Wall and WWR is barely changed compared to the low-density scenario, while Ref_Win and interactions of all design factors account for 30% and 21% of the output variation. For the HVAC demand, Ref_Wall still contributes to the highest output variation of 61%, while WWR and interactions contribute to 2% and 27% of the variation respectively. Ref_Win barely causes any change in the cooling demand. For the PV energy supply, a quite similar sensitivity result is again obtained as for the HVAC energy demand. Regarding the visual discomfort, the contribution of Ref_Wall is reduced to 46% compared with the low-density scenario, while the contribution of Ref_Win and WWR is determined as 7% and 14% respectively. In contrast with the low-density scenario, the interaction between three design parameters has been increased to 33%. It is also noteworthy that the influence of specular reflection has been obviously increased for the lighting energy demand with the increasing proximity to neighborhood buildings, which also brings about more interactive contributions to the visual discomfort. For the comparison of building performances by local sensitivity analyses as summarized in Table 4, the lighting energy demand shows no significant change with different levels of design factors, while HVAC energy demand shows a minor variation of 4.46%, which is further increased from the low-density scenario. The PV energy supply and visual discomfort time, in contrast, have been changed by up to 25.52% and 99.98% with different wall reflectance levels. In a similar study, maximum difference in the cooling energy (i.e. HVAC energy demand in this study) by changing urban design factors is up to 8% (Lima et al., 2019), which could be attributed to a different setting of envelope parameters and internal heat gains for the project building. Lighting and visual performance indicators are proved to be more sensitive to the change of urban densities as illustrated by the greater variation of sensitivity indices for the three urban design factors.

Table 4 Variation of performances in local sensitivity analysis for the medium-density scenario

	Lighting Energy Demand (kWh/m^2)	HVAC Energy Demand (kWh/m^2)	PV Energy Supply (kWh/m^2)	Visual Discomfort Time (hr)
Baseline	24.26	165.81	2.27	1011.50
Low WWR	24.29	170.72	2.65	1300.25
High WWR	24.29	161.20	1.90	1054.50
Low Ref_Win	24.60	164.41	2.14	766.75
High Ref_Win	24.06	167.46	2.41	1157.50
Low Ref_Wall	24.75	158.95	1.69	971.75
High Ref_Wall	24.05	173.21	2.85	2022.75

Solar irradiation distributions on building façades are then presented in Fig. 10 to highlight the impact of wall reflectance for the medium-density context. Incident solar radiation on the north façade is still slightly higher than that on the south façade given the same reason specified for the low-density scenario. In contrast to the low-density scenario, east and west facades show peak solar irradiance times sessions in both the morning and afternoon, indicating an increased impact from inter-building reflection with reduced distances from neighborhood developments. It can also be found that window reflectance is becoming more important for the solar harvesting potential when specular radiation also has a higher opportunity to reach the project building with a broader range of solar altitude angles.

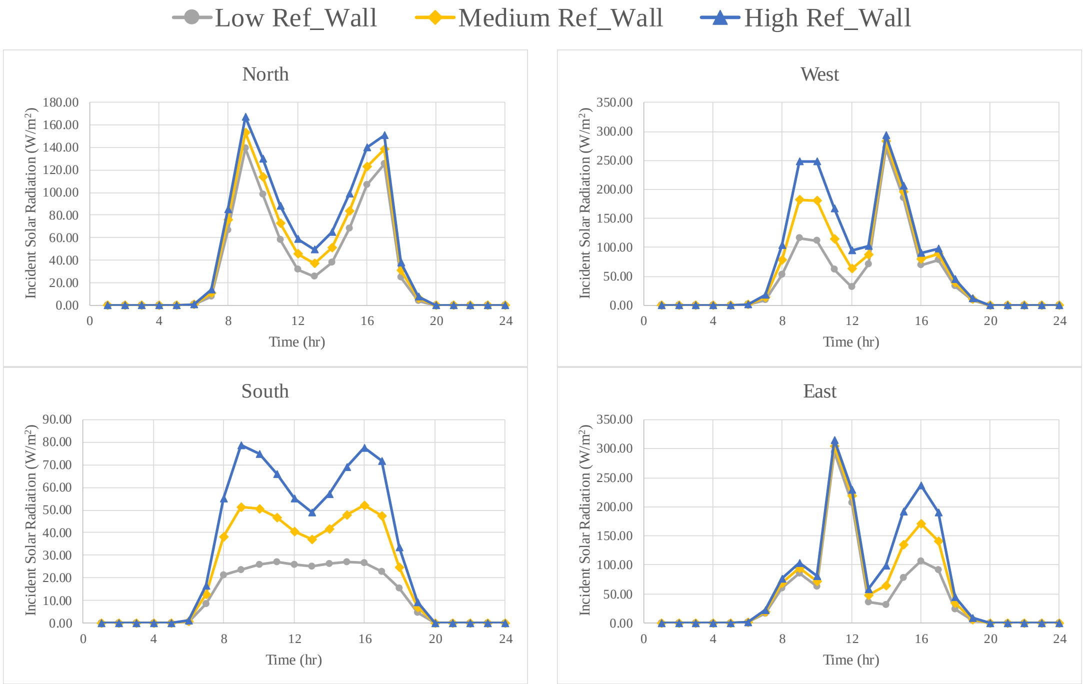

Fig. 10. Solar irradiance of project building facades for different wall reflectance of surrounding buildings with medium urban density in a selected sunny day

In the high-density urban context as shown in Fig. 11, contributions of three design factors and their interactions almost keep unchanged from the medium-density scenario. The sensitivity result for the HVAC demand is also similar to that in the medium-density scenario with a contribution from Ref_Wall, WWR and interactions of 59%, 30% and 11% respectively. For the PV energy supply, a minor increase of 4% and an equivalent decrease are observed in sensitivity indices of WWR and Ref_Wall. Regarding the visual discomfort, the contribution of Ref_Wall and WWR is reduced by 12% and 10% compared with the medium-density scenario, while the contribution of Ref_Win is increased by 7%. The contribution from interactions, however, has been further increased to 48%. As for the results from the local sensitivity analysis (See Table 5), the lighting energy demand shows a slightly increased variation up to 4.88% with different levels of design factors, while the maximum variation of the HVAC demand is reduced to 2.70%. The maximum variation of PV energy supply is increased to 46.91%, while that of the visual discomfort time is decreased to 23.66% with different wall reflectance levels. Despite the growing impact of Ref_Win with the proximity to neighborhood buildings, energy and indoor environmental performance indicators have little room for improvement as limited by available solar radiation in a highly obstructed urban environment. For instance, the increase of relative variation in PV energy supply results from the fact the average converted power is only around 0.8 kWh/m^2.

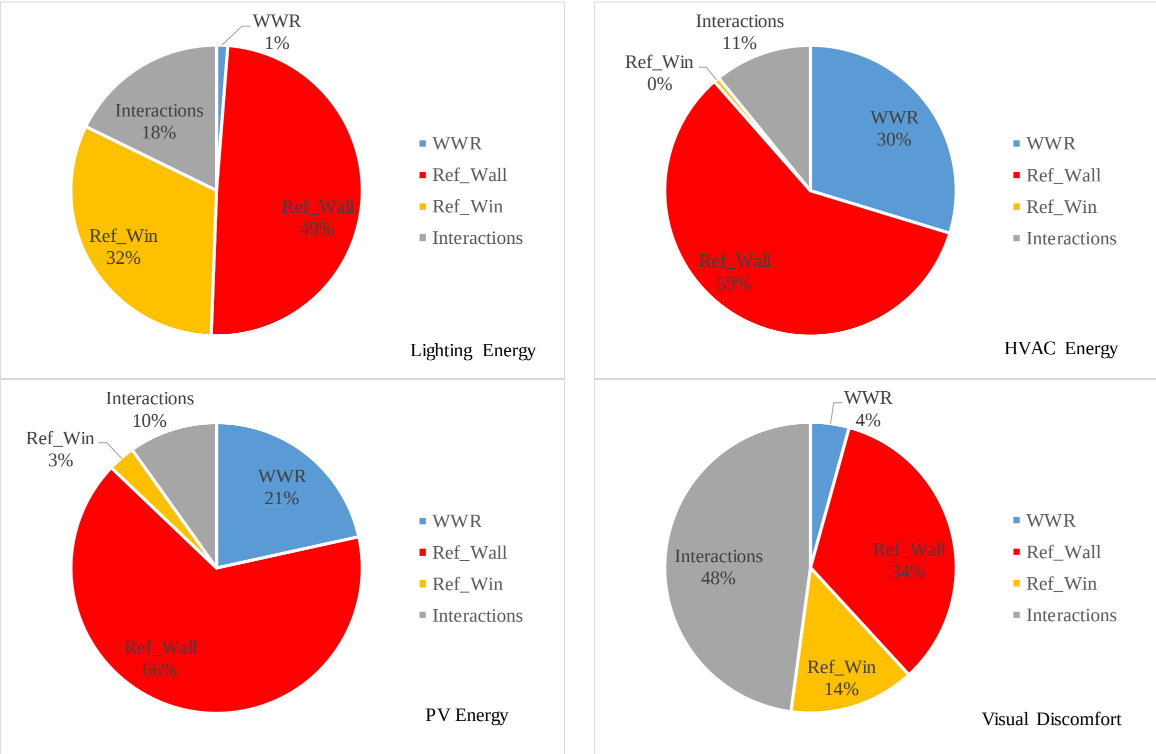

Fig. 11. Impact of peripheral building surface properties in the high-density case

Fig. 12 presents the solar irradiation distribution on each building façade to highlight the impact of wall reflectance for the high-density context. Available solar radiation is reduced on all vertical facades in this heavily obstructed urban design, therefore impairing the potential to improve project building performances. The trend of solar irradiation for north and south façades has no significant change except for a lower absolute level. However, east and west facades only show peak solar irradiance near the solar noon, which is mainly attributed to inter-building reflection from peripheral buildings. The other peak session in the medium-density scenario disappears because the lower solar angle in the morning and afternoon cannot penetrate adjacent obstructions in the high-density scenario. The influence of surface reflectance and WWR on the solar harvesting potential is proved not monotonically related to the urban density and these urban design factors are most significant in the medium-density scenario. Above findings can serve as an important design reference when coupling neighborhood planning with individual building developments.

Table 5 Variation of performances in local sensitivity analysis for the medium-density scenario

	Lighting Energy Demand (kWh/m^2)	HVAC Energy Demand (kWh/m^2)	PV Energy Supply (kWh/m^2)	Visual Discomfort Time (hr)
Baseline	29.07	153.02	0.80	224.00
Low WWR	29.19	155.79	1.03	193.00
High WWR	29.05	150.53	0.59	239.25
Low Ref_Win	29.88	152.68	0.72	171.00
High Ref_Win	28.50	153.73	0.90	241.25
Low Ref_Wall	30.49	149.79	0.43	223.50
High Ref_Wall	28.55	157.16	1.18	263.75

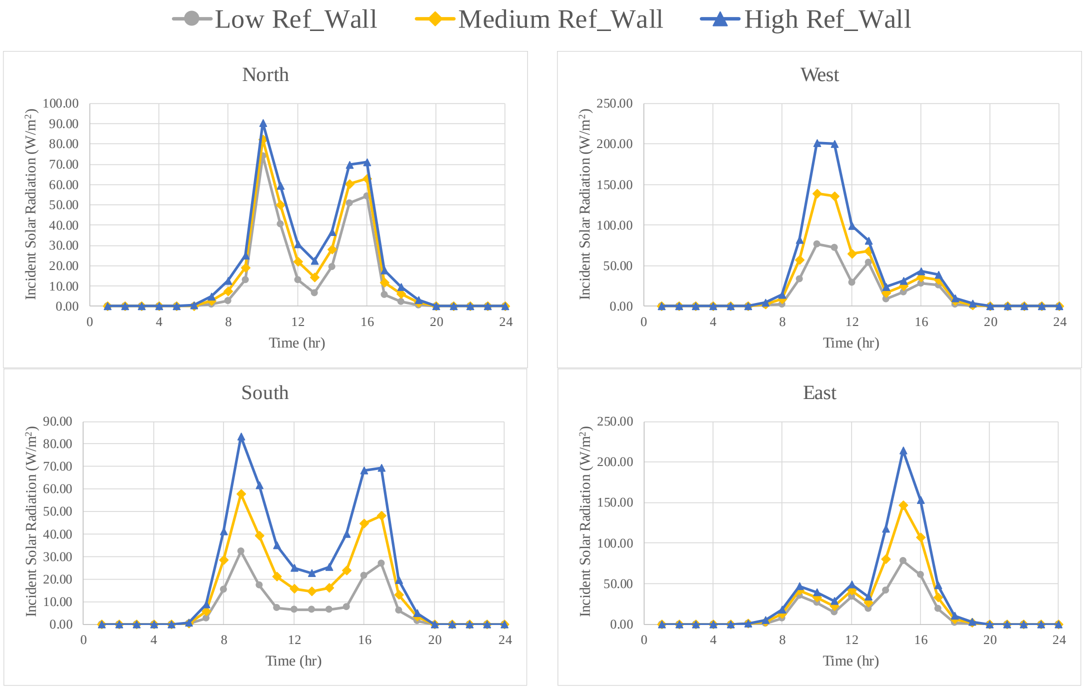

Fig. 12. Solar irradiance of project building facades for different wall reflectance of surrounding buildings with high urban density in a selected sunny day

Based on the above global sensitivity analyses for three urban design factors, Ref_Wall is determined to be the most important one contributing 34% to 66% of the variation in different performance indicators and urban density scenarios. WWR is the second important urban design factor to the variation of the HVAC energy demand and PV energy supply, while Ref_Win is generally more significant to the lighting energy demand and visual discomfort time. The influence of Ref_Win is highly dependent on solar altitude angles and proximity between buildings due to characteristics of specular reflection. The coupled impact of these urban design factors is most obvious in the medium urban context given the balance between the solar radiation availability and effectiveness of reflection. In addition, lighting and visual performance indicators are proved to be more sensitive to the change of urban densities as illustrated by the greater variation of sensitivity indices for the three urban design factors.

3.2. Sensitivity analysis for PV envelope design factors within urban context

Based on the previous sensitivity analysis, peripheral building surface properties including reflectance and the window to wall ratio are proved to have a significant influence over the energy and lighting performance of the surrounded project building in different urban densities. Although a correlation between different urban design factors and project building performances can be obtained from Table 3 to 5, it alone cannot be used as urban design guidelines. An optimum urban design can only be achieved when the overall performance of all buildings is treated as the optimization objective, echoing with existing inter-building effect analyses conducted by Han et al. (Han et al., 2017). The most appropriate selection of surface reflectance and WWR should be determined considering the trade-off between their impacts on the individual buildings and surrounding neighborhoods. This section then examines the uncertainty of PV envelope sensitivity indices regarding different neighborhood designs, where peripheral surface properties are fixed to their medium levels.

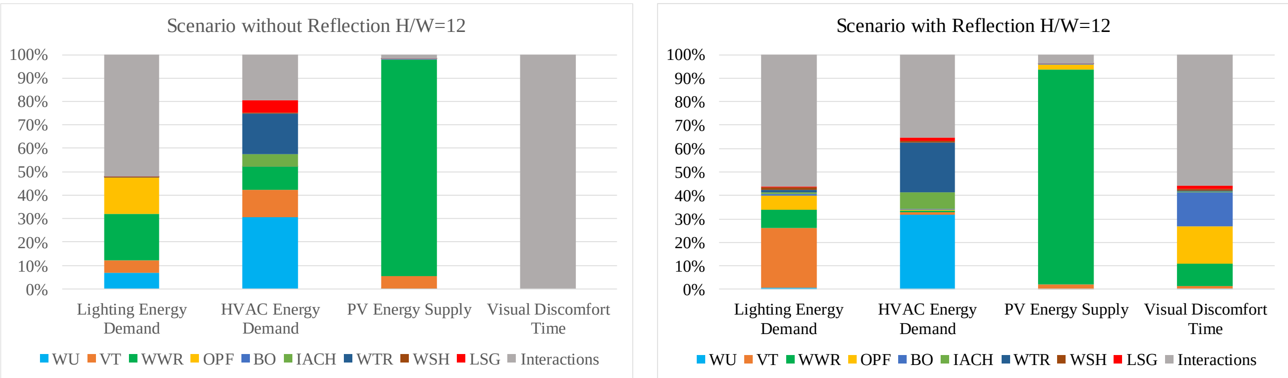

Fig. 13. Sensitivity analysis of envelope design parameters with and without surface reflectance in the high-density context

In the high-density urban context, a comparison across contributions of independent PV envelope design factors to performance indicators is summarized in Fig. 13 for modeling scenarios with and without the peripheral building surface reflectance. For the lighting energy demand considering peripheral surface reflectance, the contribution of the window to wall (WWR) and overhang projection fraction (OPF) is 19.7% and 15.7% respectively as the first and second important design parameter. The remaining envelope design parameters have little unique contributions to the output variation while the contribution of their interactions is determined to be up to 52.0%. When peripheral surface reflectance is considered, the visible transmittance (VT) of windows is determined to be the most significant design parameters with a unique contribution of 25.5% to the lighting demand. WWR and OPF together can only contribute to 14% of the output variation, while the contribution of interactions has grown to 56%. For the HVAC energy demand without peripheral surface reflectance, the window thermal property (WU) accounts for the highest output variation of 30.6%, which is followed by 17.5% contribution from the wall thermal insulation (WTR). VT and WWR rank third and fourth with sensitivity indices of 11.7% and 9.8% respectively. Interactions of all design parameters only account for 19.5% of variation in the HVAC demand. When peripheral surface reflectance is considered, only WU and WTR maintain as the top two important design parameters contributing to 31.6% and 21.4% of the output variation, while other parameters become less influential. The contribution of interactions however is increased to 35.2%. For the PV energy supply, WWR dominates influences of all design parameters with a unique contribution of 92.6% (with reflection) and 91.7% (without reflection) irrespective of the consideration of peripheral surface reflectance. For the visual discomfort without peripheral reflection, no unique contribution from design parameters can be identified because heavy obstructions from neighborhood developments have limited the solar availability and corresponding possibility of discomfort glare. However, when peripheral reflection is considered, the building orientation (BO), OPF and WWR account for 14.4%, 16.1% and 9.4% of variation in the visual discomfort time, while interactions of all design parameters still account for 56.0% of the output variation. An overall trend of increased interactive impacts from design parameters for all performance indicators can be observed when peripheral reflection is considered in the sensitivity analysis.

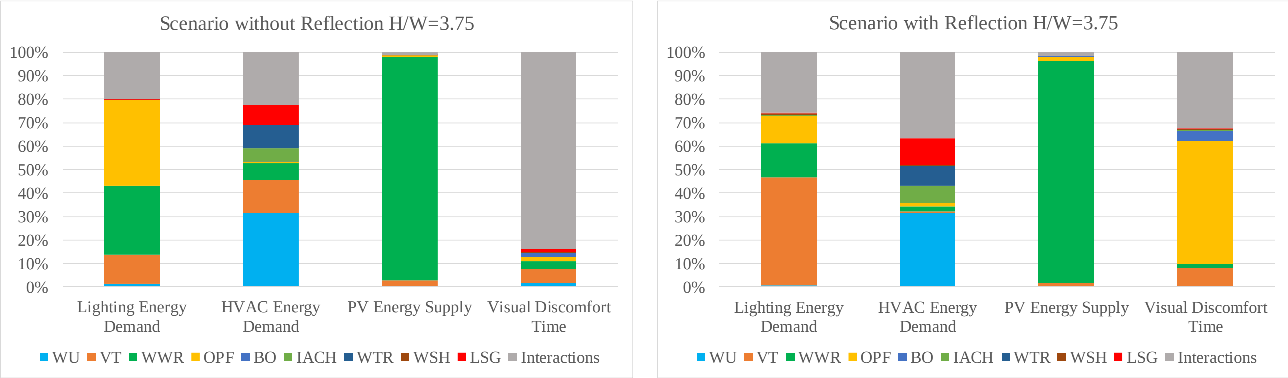

Fig. 14. Sensitivity analysis of envelope design parameters with and without surface reflectance in the medium-density context

In the medium-density urban context, the comparison of sensitivity indices for envelope design parameters with and without peripheral building surface reflectance is summarized in Fig. 14. For the lighting energy demand considering peripheral reflection, the contribution of WWR and OPF increases to 36.5% and 29.3%, where OPF becomes the most important design parameter when more solar radiation reaches less shadowed vertical facades. VT also becomes a significant design parameter with a unique contribution of 12.4%, while the contribution of their interactions is reduced to 20.1%. When peripheral reflection is considered, the impact of VT is further increased with the highest contribution of 46.2% to the lighting demand. The contribution of WWR and OPF is reduced to 14.5% and 11.5% respectively, while the contribution of interactions has grown slightly to 25.8%. For the HVAC energy demand without peripheral reflection, WU accounts for the highest output variation of 31.3% as in the high-density scenario, while VT becomes the second important design parameter with a unique contrition of 14.5%. WTR, the light-to-solar gain ratio (LSG) and WWR are ranked from third to fifth with sensitivity indices of 9.8%, 8.7% and 7.1% respectively. Interactions of all design parameters account for a slightly higher contribution of 22.4% compared to the high-density scenario. When peripheral reflection is considered, only WU and LSG maintain as the top two important design parameters contributing to 31.6% and 11.3% of the output variation, while the airtightness parameter (i.e. IACH) is ranked third with a unique contribution of 7.3%. All other design parameters become less significant and the contribution of interactions is also increased to 36.6%. For the PV energy supply, WWR still dominates influences of all design parameters with a unique contribution of 95.1% (with reflection) and 96.2% (without reflection). For the visual discomfort without peripheral reflection, only VT is identified as a significant parameter with a relatively low sensitivity index of 6.0%. When peripheral reflection is considered, the impact of OPF is greatly increased with a unique contribution of 52.6% to the visual discomfort time, while interactions of all design parameters account for 32.5% of the output variation. The observed trend of increased interactive impacts with reflection in the high-density scenario is however not identified for the visual discomfort time in the medium-density context.

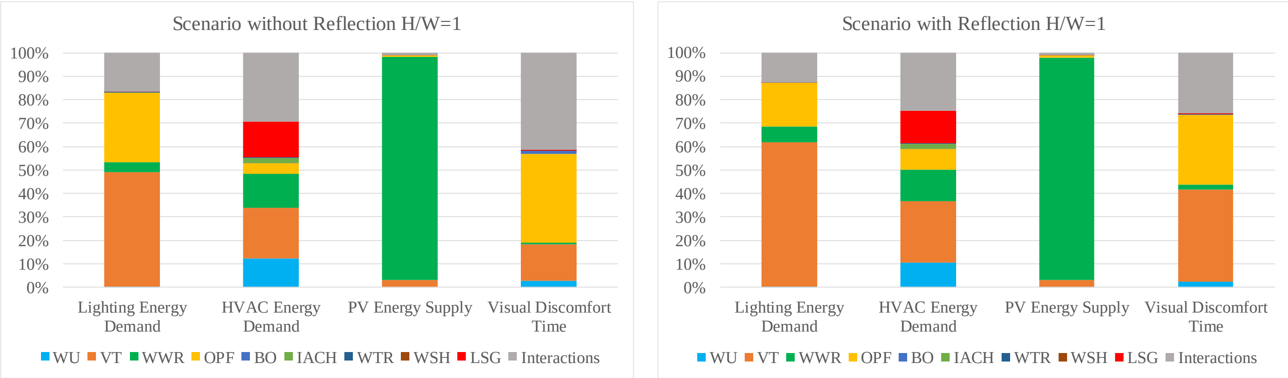

Fig. 15. Sensitivity analysis of envelope design parameters with and without surface reflectance in the low-density context

In the low-density urban context, the comparison of sensitivity results with and without peripheral building reflection is summarized in Fig. 15. For the lighting energy demand considering peripheral reflection, VT ranks first with a unique contribution of 48.6%, which is followed by OPF with a contribution of 29.8%. Daylight performance of the project building is more dependent on the visible light control of windows when peripheral shading is further reduced. The contribution of interactive impacts from all design parameters is further reduced to 16.6%. When peripheral reflection is considered, VT contributes to the highest 61.6% of the variation in the lighting demand, while the contribution of OPF and parameter interactions is reduced to 18.8% and 25.8% respectively. For the HVAC energy demand without peripheral reflection, VT has replaced WU as the most important design parameter with a unique contribution of 21.7%, which is followed by 15.0% from LSG. WWR and WU rank third and forth with sensitivity indices of 14.7% and 12.1% respectively. Interactions of all design parameters account for a slightly higher output variation of 29.4% compared to the medium-density scenario. When peripheral reflection is considered, the contribution of VT is increased to 26.3%, while that of LSG, WWR and WU is reduced to 13.6%, 13.4% and 10.4 respectively. Interactive effects of all design parameters are also reduced to 24.9%. For the PV energy supply, WWR still dominates influences of all design parameters with a unique contribution of 95.1% with and without peripheral reflection. For the visual discomfort performance without peripheral reflection, OPF and VT are identified as the two significant design parameters with sensitivity indices of 38.1% and 15.5%. When peripheral reflection is considered, the contribution of VT is increased to 39.4%, while that of OPF and interactions is reduced to 29.7% and 25.7%.

From the above comparison of sensitivity indices in different urban density scenarios with and without peripheral reflection, it can be found that interactive effects between all design parameters generally decrease with reduced urban densities for the lighting demand indicator. Inter-building reflection is proved to not only increase the computation cost in EnergyPlus but also induce statistical complexity in the factor prioritizing process except for the interpretation of the low neighborhood density scenario and visual discomfort. Window properties including the window to wall ratio (WWR), visible transmittance (VT) and overhang project fraction (OPF) are generally significant design parameters for most performance indicators, while the wall insulation (WTR), window U-value (WU) and light-to-solar gain ratio (LSG) are only important for HVAC demands. The impact of VT is generally increased for lighting performance indicators but decreased for the HVAC demand when peripheral reflection is considered. The impact of WWR, however, decreases with the consideration of peripheral reflection except for the high-density context. In addition, the impact of OPF decreases for the lighting demand with reflection while increases for the visual discomfort except in the low-density context. Such uncertainty analyses on envelope design sensitivity indices are seldom observed in existing studies and should be part of the originality in this research.

3.3. Multicriteria decision-making for integrated building envelope design

A multi-criterion design optimization of the PV envelope is then conducted for different neighborhood densities considering peripheral surface reflectance. NSGA-II achieved convergence within 1820 model evaluations for different urban density scenarios and generated up to 616 Pareto optimal solutions (as shown in Fig. 16). As contradictive or synergetic relationships between optimization objectives can be observed from these solutions, decision-making strategies are required to find out the final solution. The minimum distance to the Utopia point method (MDUP) is first applied to Pareto optimal solutions and the single optimum solution closest to the ideal point is identified. Each normalized optimization objective/performance indicator is weighted equally in this decision-making approach, whereas diverse weightings could be considered in a real decision-making process to reflect preferences of different stakeholders. The TOPSIS (Technique for Order of Preference by Similarity to Ideal Solution) method is therefore applied to allocate priorities to performance indicators. Considering the popularity of incorporating green building design guidelines to early-stage building designs, three weighting systems are integrated with TOPSIS: Equivalent weighting (i.e. TOPSIS1), BEAM criteria based weighting (i.e. TOPSIS2), and LEED criteria based weighting (i.e. TOPSIS3). The optimum solution is recommended based on the proximity between optimum solutions under different decision-making approaches and the ideal solution (i.e. [0, 0] in when normalized) on two dimensional charts with different pairs of optimization criteria.

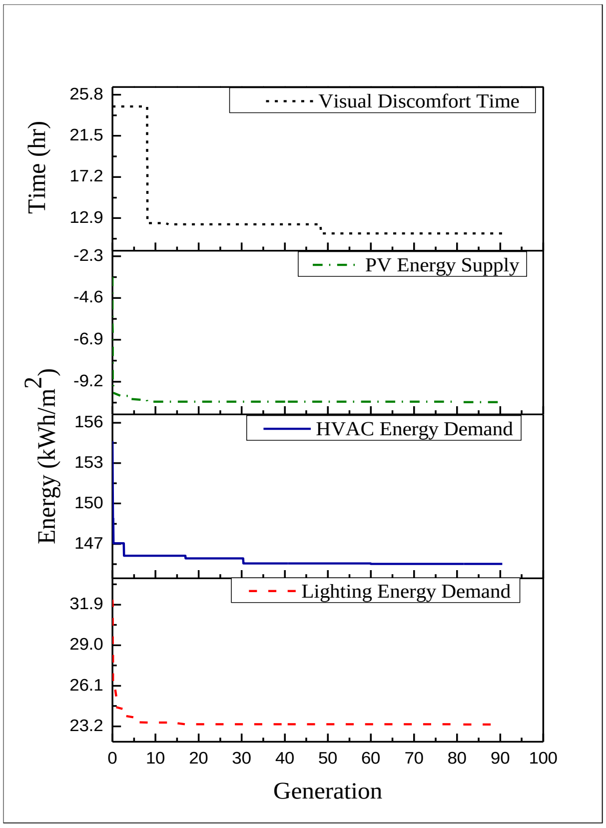

Fig. 16 Convergence chart of multicriteria optimization (Medium-density case)

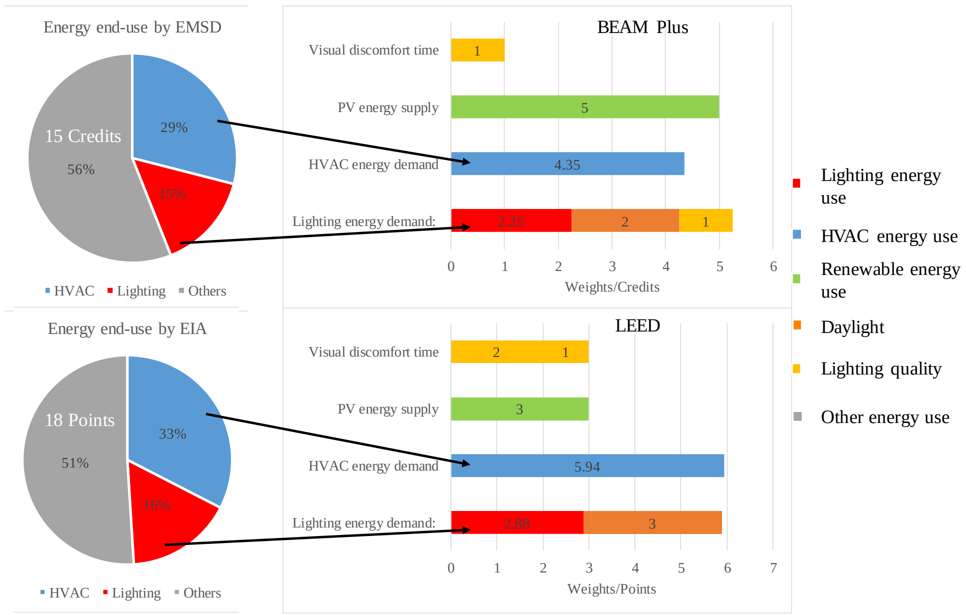

Fig. 17. Demonstration of LEED and BEAM criteria based weighting systems

Fig. 17 illustrates the method to construct two weighting systems based on green building assessment schemes. For both systems, all relevant credits/points in the energy and indoor environment quality (IEQ) category of assessment schemes are examined for the four performance indicators. The total applicable credit for each performance indicator is used as its weighting in the optimization process. Taking the BEAM Plus system as an example, the total available credit for the annual energy use criterion is 15, which is decomposed based on official building energy end-use statistics to calculate lighting and HVAC energy related credits. The 4.35 credit is then used as the weighting for HVAC energy demand, while the 2.25 credit is combined with other relevant credits for the lighting energy demand. Two credits in the daylight and 1 credit in the lighting quality (i.e. daylight sensor) criterion are related to the lighting energy calculation based on the applied dimming control and daylight illuminance threshold in the building model. As a result, the total available credit for the lighting demand is 5.25. 5 credits are granted to renewable applications covering up to 2.5% of the total building energy consumption, so that it is adopted directly as the weighting for the PV energy supply. 1 credit concerning the glare issue from lighting quality criteria is granted as the weighting for the visual discomfort time. In summary, a weighting system of {5.25, 4.35, 5, 1} is applied to TOPSIS for decision-making.

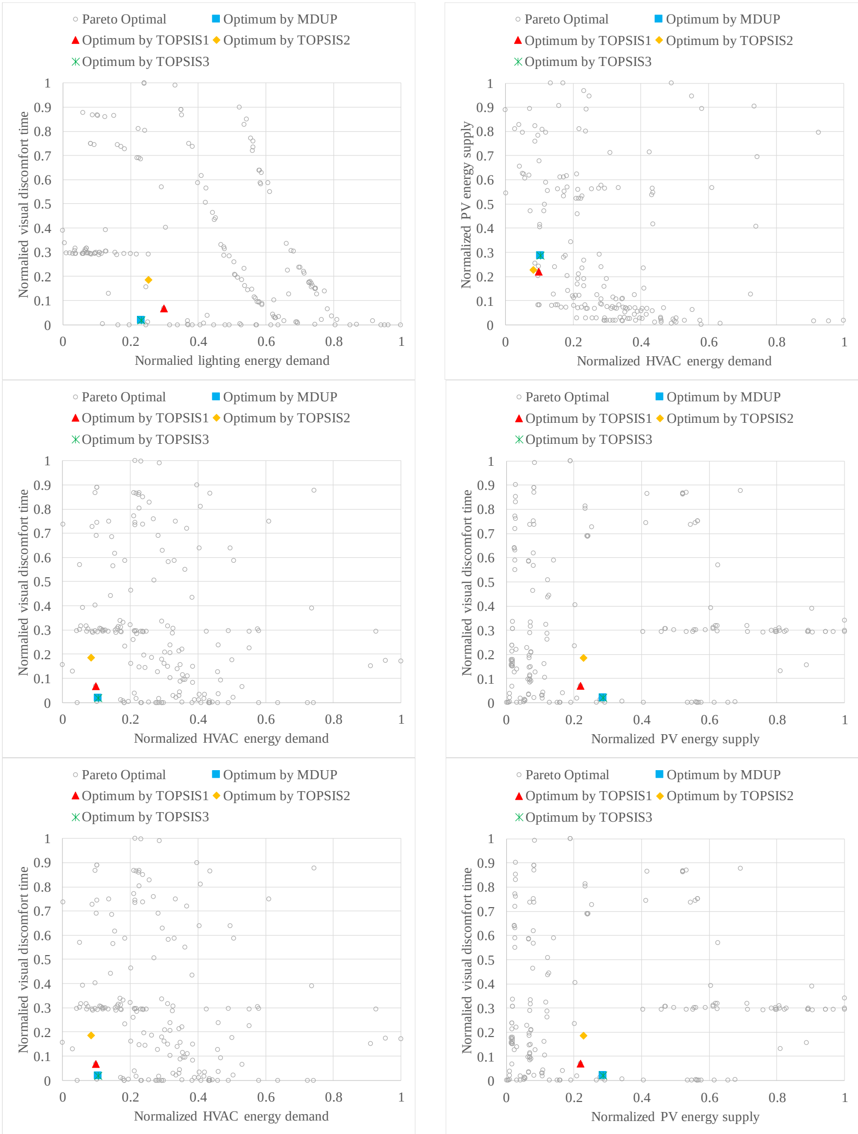

Fig. 18. Comparing integrated optimization and decision-making for the high-density context

The comparison of different decision-making approaches is presented in Fig. 18 for the high-density context. The optimum solution obtained from TOPSIS with LEED criteria based weightings (TOPSIS3) has the same minimum distance to the ideal solution as that obtained from MDUP. Based on the frequency where different solutions are closest to the ideal solution in two-dimensional charts, the second best solution should be from TOPSIS1 based on the equal weighting system. The optimum solution for the high-density urban context with peripheral reflection can achieve a net building energy demand of 168.28 kWh/m^2 and an average visual discomfort time of 0.69 hours over perimeter zones. The optimized design is characterized by a high visible transmittance (VT) of 0.86 and a high window U-value (WU) of 4.68 W/m^2·K. Its window to wall ratio (WWR), wall thermal resistance (WTR), overhang projection fraction (OPF) and light-to-solar gain ratio are all set to a relatively low level of 0.26, 0.09, 0.17 m^2·K/W and 1.49.

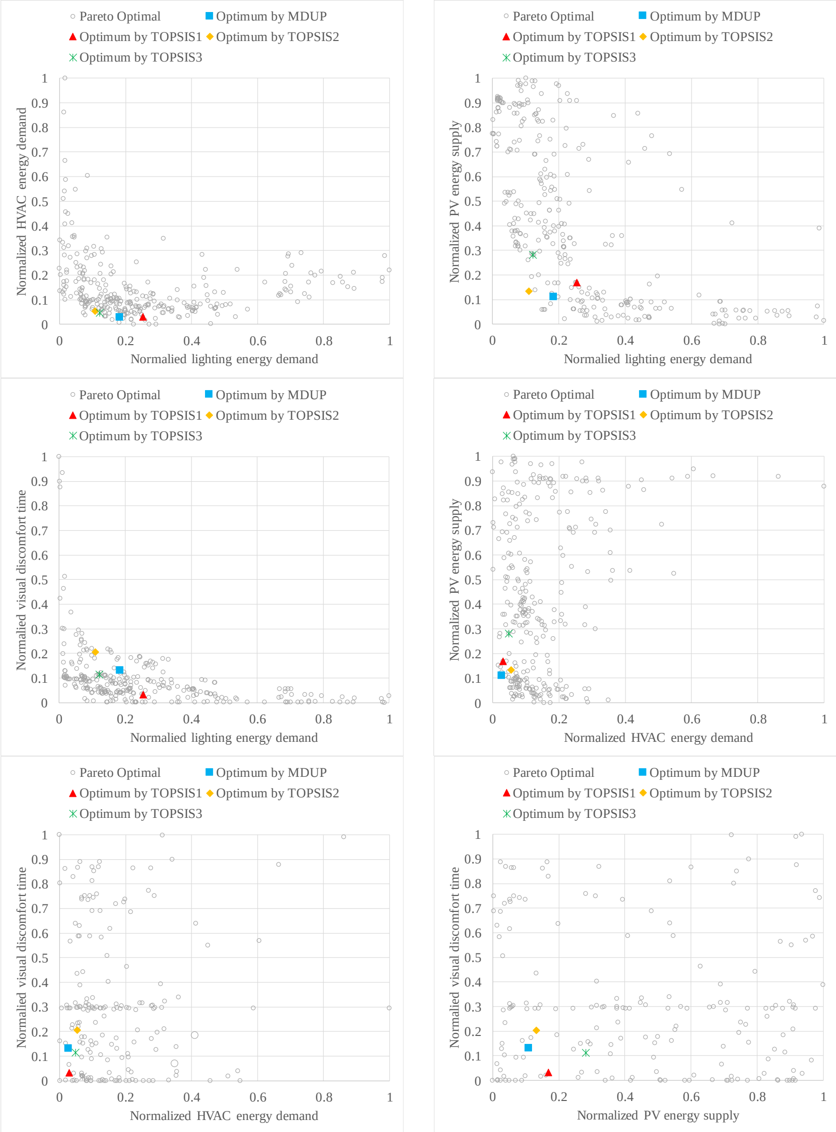

Fig. 19. Comparing integrated optimization and decision-making for the medium-density context

Fig. 19 compares different decision-making approaches for the medium-density context, where clear trade-offs can be observed between the lighting and HVAC demand as well as the lighting demand and visual discomfort time. The optimum solution obtained from TOPSIS with BEAM criteria based weightings (TOPSIS2) is ranked equally with optimum solution obtained from MDUP based on the number of times they are closest to the ideal solution in two-dimensional charts (Mangkuto et al., 2016). The two optimum solutions for the medium-density urban context with peripheral reflection can achieve a net building energy demand of 161.83~162.17 kWh/m^2 and an average visual discomfort time of 161.81~247.31 hours over perimeter zones. The major change in the design space compared to high-density scenarios lies in the setting of LSG, which has been increased to a high level of 2.25 in the solution from MDUP to control the thermal load without impairing the utilization of natural lighting.

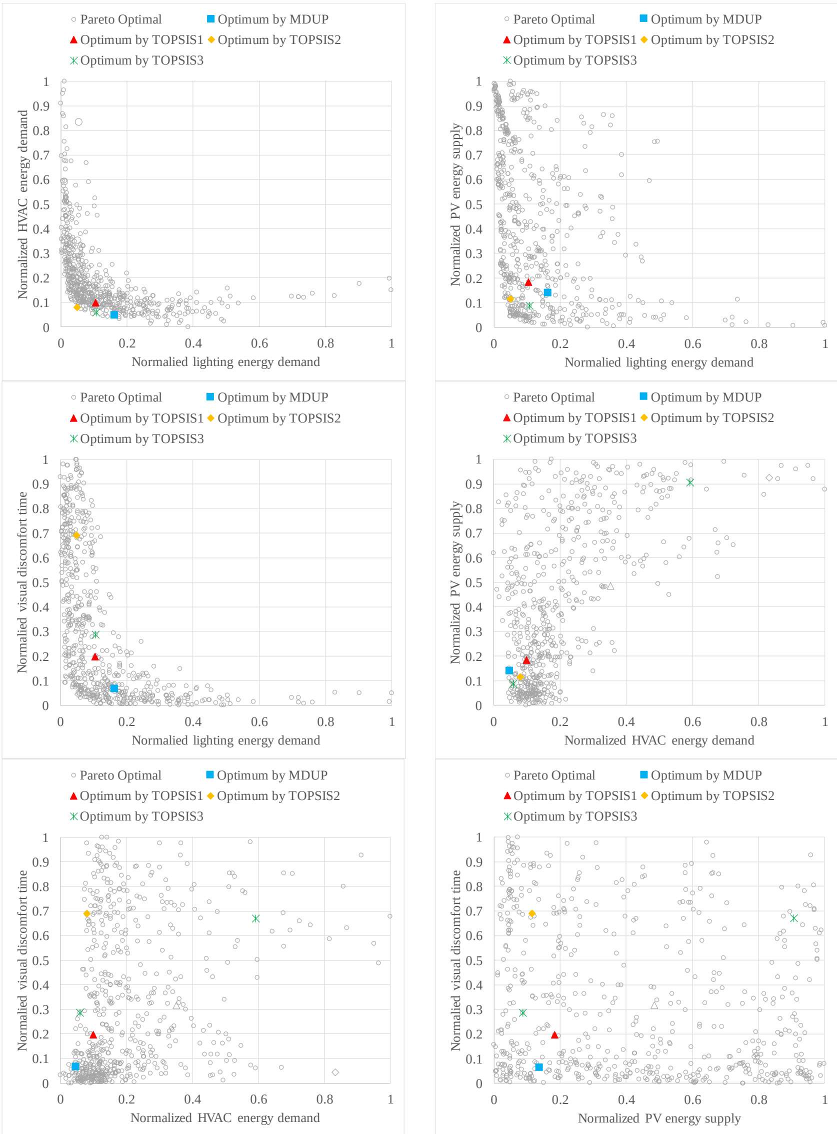

Fig. 20. Comparing integrated optimization and decision-making for the high-density context

In the low-density scenario, the optimum solution obtained from TOPSIS with BEAM criteria based weightings (TOPSIS2) is closest to the optimum solution obtained from MDUP based on their proximity to the ideal solution in two-dimensional charts as per Fig. 20. MDUP is therefore determined to be the most suitable decision-making strategy for integrated PV envelope optimization in such an urban context. Similar trade-offs between optimization objectives can also be observed as in the medium-density scenario. The optimum solution for the low-density urban context with peripheral reflection can achieve a net building energy demand of 154.15 kWh/m^2 and an average visual discomfort time of 215.19 hours over perimeter zones. A major deviation from the other two urban contexts is identified in VT, which is reduced to 0.32 to control discomfort glare in a less obstructed peripheral environment.

Table 6 Optimum solutions for most suitable decision-making methods in different urban contexts

	High-density context	Medium-density context		Low-density context
	TOPSIS3/ MDUP	***TOPSIS2***	***MDUP***	***MDUP***
BO (°)	171	144	82	86
WSH (J/kg·K)	1054	1993	1773	1036
VT	0.86	0.83	0.74	0.32
WTR (m^2·K/W)	0.17	0.33	0.12	0.61
LSG	1.49	1.21	2.25	1.52
WWR	0.26	0.16	0.14	0.23
WU (W/m^2·K)	4.68	4.68	3.76	3.94
OPF	0.09	0.14	0.08	0.02
IACH (h^{-1})	1.35	1.47	1.47	1.46
Lighting energy demand (kWh/m^2)	26.47	24.28	24.93	23.53
HVAC energy demand (kWh/m^2)	144.87	147.07	146.29	148.29
PV energy supply (kWh/m^2)	3.06	9.19	9.39	17.67
Total net energy demand (kWh/m^2)	168.28	162.17	161.83	154.15
Visual discomfort time (hr)	0.69	247.31	161.81	215.19

All performance indicators and envelope design parameters for optimum solutions within different urban contexts are summarized in Table 6. A general decrease of the lighting, HVAC demand and PV power generation can be clearly identified when compared with solutions in a previous single-objective (i.e. net building energy demand) optimization study without considering peripheral reflection (Chen et al., 2019b). The total optimized net building energy demand is reduced by up to 8.84% owing to 76.13% increased PV power generation and 24.28% reduced lighting demand within the medium-density context. Such differences can be attributed to solar reflection from neighborhood envelopes and applied multi-criterion decision-making approaches, which validated the necessity and significance of integrating inter-building effect with building design optimizations. By comparing the TOPSIS method with the previously used MDUP method, it can be found that the proposed decision-making approach can generate robust optimum solutions with an equivalent proximity to the ideal solution while addressing the preference of stakeholders and green building design guidelines.

4. Conclusions

This article presented a comparative sensitivity and design optimization study on integrated PV envelope systems considering peripheral surface reflection and neighborhood densities. Both uncertainty and sensitivity analyses are conducted with EnergyPlus and R to quantify the contribution of key design parameters and their impact on energy and indoor environment performance indicators within miscellaneous combinations of urban design factors. Multi-criterion optimizations coupled with proposed decision-making strategies are also compared and discussed to obtain optimum building envelope designs for typical high-rise commercial buildings. Major findings are detailed as below:

1) Building performance indicators related to PV envelope designs are comprehensively investigated and deeply coupled with green building assessment schemes in this research. The lighting energy demand is derived from the daylight calculation and dimming control algorithm based on illumination thresholds, which address both energy use and natural lighting aspects in green building design guidelines. Cooling, heating and ventilation loads are summarized under the HVAC demand, where indoor thermal comfort is assumed to be satisfied with an ideal system. PV energy supply is used to quantify the solar energy harvesting potential and address renewable energy utilization requirements, while the visual discomfort time is calculated based on the glare index to fulfill lighting quality requirements.
2) Variance-based sensitivity analyses are conducted for urban design factors including the window to wall ratio (WWR), wall surface reflectance (Ref_Wall), and window surface reflectance (Ref_Win) of peripheral buildings. Ref_Wall is determined to be the most important urban design factor contributing 34% to 66% of the variation in different performance indicators and urban density scenarios. WWR is the second important urban design factor to the variation of the HVAC energy demand and PV energy supply, while Ref_Win is generally more significant to the lighting energy demand and visual discomfort time. The influence of Ref_Win is highly dependent on solar altitude angles and proximity between buildings due to characteristics of specular reflection. The coupled impact of these urban design factors is most obvious in the medium urban context given the balance between the solar radiation availability

and effectiveness of reflection.

3) In light of the significance of the inter-building effect from urban design factors, the uncertainty of sensitivity indices for PV envelope design parameters is examined with all peripheral building surface properties fixed to their medium levels. It can be found that peripheral surface reflection can increase interactive effects between design parameters for the lighting and HVAC energy demands in higher density contexts. Sensitivity indices for the visual discomfort time are subject to the greatest variation when peripheral reflection is considered, while those for the PV energy supply are almost maintained constant. Window properties including the window to wall ratio (WWR), visible transmittance (VT) and overhang project fraction (OPF) are generally significant design parameters for most performance indicators, while the wall insulation (WTR), window U-value (WU) and light-to-solar gain ratio (LSG) are only important for HVAC demands.
4) Multi-criterion optimizations with NSGA-II are conducted for different urban densities considering peripheral reflection. Trade-offs between the HVAC and lighting demand as well as between the lighting demand and visual discomfort time are clearly identified from Pareto optimal solutions in medium and low density contexts. Regarding the post decision-making process, the proposed TOPSIS (Technique for Order of Preference by Similarity to Ideal Solution) method integrated with different weighting schemes can generate robust optimum solutions based on a comparison with MDUP (Minimum Distance to the Utopia Point) on two-dimensional charts of paired optimization criteria. The integrated design optimization considering peripheral reflection can vary the optimal net energy demand by up to 8.84%, attributed to great changes in the PV supply and lighting demand.
5) In addition, this integrated design optimization with TOPSIS based on different weightings can also sufficiently reflect preferences of diverse stakeholders and green building assessment requirements. Considering the trend of incorporating green building design guidelines into early-stage building designs and urban planning, this study can contribute to further integration of synergetic energy and indoor environment design strategies with expanded applications of renewable systems.

Acknowledgment

The work described in this paper was supported by the Innovation and Technology Fund with project No. ITS/171/16FX and the Postdoctoral Fellow Scheme of the Faculty of Construction and Environment, The Hong Kong Polytechnic University (Grant No.: K-ZM2G).

Nomenclatures

Abbreviation

ANOVA	analysis of variance
BEAM	building environment assessment method
BIPV	building integrated photovoltaic
BO	building orientation
FAST	Fourier amplitude sensitivity test
GPVA	active glazing PV area
HVAC	heating ventilation and air conditioning
IACH	infiltration air change per hour
IBE	inter-building effect
IEQ	indoor environment quality
IWEC	international weather for energy calculations
LEED	leadership in energy and environmental design
LSG	light to solar gain ratio
MUDP	minimum distance to the utopia point
NSGA-II	non-dominated sorting genetic algorithm-II
OPF	overhang projection fraction
PV	photovoltaic
Ref_Wall	wall surface reflectance
Ref_Win	window surface reflectance
SA	sensitivity analysis
SHGC	solar heat gain coefficient
TOPSIS	technique for order of preference by similarity to ideal solution
VT	visible transmittance
WGR	window to ground ratio
WPVA	active wall PV area
WSH	wall specific heat
WTR	wall thermal resistance
WU	window U-value
WWR	window to wall ratio

References

2013. ASHARE 90.1: Energy Standard for Buildings Except Low-Rise Residential Buildings. ASHRAE.

Allegrini, J., Dorer, V., Carmeliet, J., 2016. Impact of radiation exchange between buildings in urban street canyons on space cooling demands of buildings. Energy and Buildings 127, 1074-1084.

Baldi, S., Karagevrekis, A., Michailidis, I.T., Kosmatopoulos, E.B., 2015. Joint energy demand and thermal comfort optimization in photovoltaic-equipped interconnected microgrids. Energy Conversion and Management 101, 352-363.

BEAM, 2012. BEAM Plus New Buildings Version 1.2. HKGBC and BEAM Society Limited.

Burg, B.R., Ruch, P., Paredes, S., Michel, B., 2017. Effects of radiative forcing of building integrated photovoltaic systems in different urban climates. Solar Energy 147, 399-405.

Cha, L.H., Bhang, G.B., Park, Y.S., Choi, H.J., Ahn, K.H., 2018. Power Prediction of Bifacial Si PV Module with Different Reflection Conditions on Rooftop. Applied Sciences 8.

Chan, A.L.S., 2018. Evaluating the impact of photovoltaic systems on the thermal performance of buildings and its implication to building energy code. A case study in subtropical Hong Kong. Energy Policy 119, 674-688.

Chan, A.L.S., Chow, T.T., Fong, K.F., Lin, Z., 2009. Investigation on energy performance of double skin façade in Hong Kong. Energy and Buildings 41, 1135-1142.

Chen, X., Huang, J., Yang, H., Peng, J., 2019a. Approaching low-energy high-rise building by integrating passive architectural design with photovoltaic application. Journal of Cleaner Production 220, 313-330.

Chen, X., Yang, H., Peng, J., 2019b. Energy optimization of high-rise commercial buildings integrated with photovoltaic facades in urban context. Energy 172, 1-17.

Chen, X., Yang, H., Sun, K., 2017a. Developing a meta-model for sensitivity analyses and prediction of building performance for passively designed high-rise residential buildings. Applied Energy 194, 422-439.

Chen, X., Yang, H., Wang, T., 2017b. Developing a robust assessment system for the passive design approach in the green building rating scheme of Hong Kong. Journal of Cleaner Production 153, 176-194.

Chen, X., Yang, H., Zhang, W., 2018. Simulation-based approach to optimize passively designed buildings: A case study on a typical architectural form in hot and humid climates. Renewable and Sustainable Energy Reviews 82, 1712-1725.

Chen, Y., Hong, T., 2018. Impacts of building geometry modeling methods on the simulation results of urban building energy models. Applied Energy 215, 717-735.

Connelly, K., Wu, Y., Ma, X., Lei, Y., 2017. Transmittance and Reflectance Studies of Thermotropic Material for a Novel Building Integrated Concentrating Photovoltaic (BICPV) 'Smart Window' System. Energies 10.

Cukier, R.I., Levine, H.B., Shuler, K.E., 1978. Nonlinear sensitivity analysis of multiparameter model systems. Journal of Computational Physics 26, 1-42.

Delgarm, N., Sajadi, B., Kowsary, F., Delgarm, S., 2016. Multi-objective optimization of the building energy performance: A simulation-based approach by means of particle swarm optimization (PSO). Applied Energy 170, 293-303.

EMSD, 2018. Hong Kong Energy End-use Data 2018. Electrical & Mechanical Services Department. http://www.emsd.gov.hk.

Gueymard, C.A., duPont, W.C., 2009. Spectral effects on the transmittance, solar heat gain, and performance rating of glazing systems. Solar Energy 83, 940-953.

Han, Y., Taylor, J.E., Pisello, A.L., 2017. Exploring mutual shading and mutual reflection inter-building effects on building energy performance. Applied Energy 185, Part 2, 1556-1564.

Huang, J., Chen, X., Yang, H., Zhang, W., 2018. Numerical investigation of a novel vacuum photovoltaic curtain wall and integrated optimization of photovoltaic envelope systems. Applied Energy 229, 1048-1060.

Huang, K.-T., Li, Y.-J., 2017. Impact of street canyon typology on building's peak cooling energy demand: A parametric analysis using orthogonal experiment. Energy and Buildings 154, 448-464.

Konis, K., Gamas, A., Kensek, K., 2016. Passive performance and building form: An optimization framework for early-stage design support. Solar Energy 125, 161-179.

Lam, J.C., 2000. Shading effects due to nearby buildings and energy implications. Energy Conversion and Management 41, 647-659.

Lam, J.C., Chan, R.Y.C., Tsang, C.L., Li, D.H.W., 2004. Electricity use characteristics of purpose-built office buildings in subtropical climates. Energy Conversion and Management 45, 829-844.

Lee, C., Won, J., 2017. Analysis of combinations of glazing properties to improve economic efficiency of buildings. Journal of Cleaner Production 166, 181-188.

Li, D.H.W., Wong, S.L., Tsang, C.L., Cheung, G.H.W., 2006. A study of the daylighting performance and energy use in heavily obstructed residential buildings via computer simulation techniques, Energy and Buildings, pp. 1343-1348.

Lima, I., Scalco, V., Lamberts, R., 2019. Estimating the impact of urban densification on high-rise office building cooling loads in a hot and humid climate. Energy and Buildings 182, 30-44.

Lu, M., Du, J., 2019. Dynamic Evaluation of Daylight Availability in a Highly-dense Chinese Residential Area with a Cold Climate. Energy and Buildings.

Mangkuto, R.A., Rohmah, M., Asri, A.D., 2016. Design optimisation for window size, orientation, and wall reflectance with regard to various daylight metrics and lighting energy demand: A case study of buildings in the tropics. Applied Energy 164, 211-219.

Martins, T.A.d.L., Adolphe, L., Bastos, L.E.G., Martins, M.A.d.L., 2016. Sensitivity analysis of urban morphology factors regarding solar energy potential of buildings in a Brazilian tropical context. Solar Energy 137, 11-24.

Martins, T.A.d.L., Faraut, S., Adolphe, L., 2019. Influence of context-sensitive urban and architectural design factors on the energy demand of buildings in Toulouse, France. Energy and Buildings.

Marzouk, M., Azab, S., Metawie, M., 2018. BIM-based approach for optimizing life cycle costs of sustainable buildings. Journal of Cleaner Production 188, 217-226.

Nabil, A., Mardaljevic, J., 2006. Useful daylight illuminances: A replacement for daylight factors. Energy and Buildings 38, 905-913.

Pal, S.K., Takano, A., Alanne, K., Palonen, M., Siren, K., 2017. A multi-objective life cycle approach for optimal building design: A case study in Finnish context. Journal of Cleaner Production 143, 1021-1035.

Peng, J., Curcija, D.C., Lu, L., Selkowitz, S.E., Yang, H., Mitchell, R., 2016. Developing a method and simulation model for evaluating the overall energy performance of a ventilated semi-transparent photovoltaic double-skin facade. Progress in Photovoltaics: Research and Applications 24, 781-799.

Sadineni, S.B., Madala, S., Boehm, R.F., 2011. Passive building energy savings: A review of building envelope components. Renewable and Sustainable Energy Reviews 15, 3617-3631.

Saltelli, A., Tarantola, S., Chan, K.P.S., 1999. A Quantitative Model-Independent Method for Global Sensitivity Analysis of Model Output. Technometrics 41, 39-56.

Samuelson, H., Claussnitzer, S., Goyal, A., Chen, Y., Romo-Castillo, A., 2016. Parametric energy simulation in early design: High-rise residential buildings in urban contexts. Building and Environment 101, 19-31.

Selj, J.H., Mongstad, T.T., Søndenå, R., Marstein, E.S., 2011. Reduction of optical losses in colored solar cells with multilayer antireflection coatings. Solar Energy Materials and Solar Cells 95, 2576-2582.

Shen, P., Dai, M., Xu, P., Dong, W., 2019. Building heating and cooling load under different neighbourhood forms: Assessing the effect of external convective heat transfer. Energy 173, 75-91.

Wang, M., Peng, J., Li, N., Yang, H., Wang, C., Li, X., Lu, T., 2017. Comparison of energy performance between PV double skin facades and PV insulating glass units. Applied Energy 194, 148-160.

Yu, P.C.H., Chow, W.K., 2001. Energy use in commercial buildings in Hong Kong. Applied Energy 69, 243-255.

Zhang, A., Bokel, R., van den Dobbelsteen, A., Sun, Y., Huang, Q., Zhang, Q., 2017. Optimization of thermal and daylight performance of school buildings based on a multi-objective genetic algorithm in the cold climate of China. Energy and Buildings 139, 371-384.

Zhang, J., Xu, L., Shabunko, V., Tay, S.E.R., Sun, H., Lau, S.S.Y., Reindl, T., 2019. Impact of urban block typology on building solar potential and energy use efficiency in tropical high-density city. Applied Energy 240, 513-533.

Zhang, T.T., Tan, Y.F., Yang, H.X., Zhang, X.D., 2016a. The application of air layers in building envelopes: A review. Applied Energy 165, 707-734.

Zhang, W., Lu, L., Peng, J., Song, A., 2016b. Comparison of the overall energy performance of semi-transparent photovoltaic windows and common energy-efficient windows in Hong Kong. Energy and Buildings 128, 511-518.